Graphene-Perovskite Fibre Photodetectors

*S. Akhavan, A. Taheri Najafabadi, S. Mignuzzi, M. Abdi Jalebi, A. Ruocco, I. Paradisanos, O. Balci, Z. Andaji-Garmaroudi, I. Goykhman, L. G. Occhipinti, E. Lidorikis, S. D. Stranks, and A. C. Ferrari**

The integration of optoelectronic devices, such as transistors and photodetectors (PDs), into wearables and textiles is of great interest for applications such as healthcare and physiological monitoring. These require flexible/wearable systems adaptable to body motions, thus materials conformable to non-planar surfaces, and able to maintain performance under mechanical distortions. Here, fibre PDs are prepared by combining rolled graphene layers and photoactive perovskites. Conductive fibres (~500 Ωcm^{-1}) are made by rolling single-layer graphene (SLG) around silica fibres, followed by deposition of a dielectric layer (Al_2O_3 and parylene C), another rolled SLG as a channel, and perovskite as photoactive component. The resulting gate-tunable PD has a response time~9ms, with an external responsivity~22kAW^{-1} at 488nm for a 1V bias. The external responsivity is two orders of magnitude higher, and the response time one order of magnitude faster, than state-of-the-art wearable fibre-based PDs. Under bending at 4mm radius, up to~80% photocurrent is maintained. Washability tests show~72% of initial photocurrent after 30 cycles, promising for wearable applications.

1. Introduction

Electronics on fibres and textiles is of great interest for applications including healthcare (e.g., monitoring heart rate),[1] wearable displays,[2] energy harvesting,[3,4] and storage.[5] The current vision for electronic textiles is for them to be an integral part of our everyday outfits,[6,7] and remain functional after washing.[8]

One of the most common approaches to test the washability of e-textiles was developed by the American Association of Textile Chemists and Colorists (AATCC).[9] One cycle in AATCC is equivalent to five regular-machine (household) washing cycles,[10] achieved by the addition of steel or rubber balls to the washing container,[10] with agitator speed 179±2 spm and spin speed 645±15 rpm.[9] Washability tests are performed for at least 20 cycles,[10] with each cycle being 45 min at 40 °C, with ~0.37% volume of detergent (AATCC standard reference detergent 124),[9] and ten stainless steel balls (6 mm) or load ballast (130±10 g for cotton) to mimic abrasion.[9,11] The analysis of washability depends on the intended application, the expected frequency of cleaning, and the total number of cleaning cycles during the tested product's lifetime. E.g., sports clothing will be mainly washed after every use,[12] while a jacket will only be cleaned once or twice a year.[10,13]

Bendability can be achieved by integrating rigid components (e.g., Si-based)[14] within flexible systems,[15] including textiles.[16] However, device rigidity (i.e., intolerance to various forms of mechanical stress caused by body motions),[17] and washability issues,[18] are bottlenecks for commercialization.[6] Additionally, wafer-based manufacturing processes are generally optimized for planar fabrication[19] and substrates.[20]

S. Akhavan[+], A. T. Najafabadi[++], S. Mignuzzi, A. Ruocco,
I. Paradisanos, O. Balci, I. Goykhman, L. G. Occhipinti, A. C. Ferrari
Cambridge Graphene Centre
University of Cambridge
JJ Thompson Avenue, Cambridge CB3 0FA, UK
E-mail: acf26@eng.cam.ac.uk

[+]Present address: Institute for Materials Discovery, University College London, Torrington Place, London WC1E 7JE, UK

[++]Present address: Faculty of Engineering and Science, University of Greenwich, Central Avenue, Chatham Maritime, Kent ME4 4TB, UK

M. A. Jalebi[+], Z. Andaji-Garmaroudi
Cavendish Laboratory
University of Cambridge
JJ Thompson Avenue, Cambridge CB3 0HE, UK

A. Ruocco
Optical Networks Group
University College London
London WC1E 6BT, UK

I. Goykhman
Technion - Israel Institute of Technology
Haifa 3200003, Israel

E. Lidorikis
Department of Materials Science and Engineering
University of Ioannina
Ioannina 45110, Greece

S. D. Stranks
Department of Chemical Engineering and Biotechnology
University of Cambridge
Philippa Fawcett Drive, Cambridge CB3 0AS, UK

Table 1. Comparison of KPIs for PDs on rigid and flexible substrates. PA: polyamide. NA: not applicable. ND: not defined. The last three rows are neither PDs nor fibre-based structures. Ref. [40] reported 3.5 times higher resistance ($\approx$700 Ωcm^{-1}) after ten washing cycles. Ref. [40] reported 10 home laundry washing cycles by following a British Standard (BS EN ISO 105 C06 A1S). Ref. [41] measured ~80% of the initial power conversion efficiency after submersion in water. Ref. [74] had ~50% drop in drain current after 20 washing cycles. Our fibre-based PDs maintain up to ~72% I_{ph} after 30 AATCC washing cycles.

Structure (Substrate)[Refs.]	Properties						
	R_{ext} [A/W]	Spectral range [nm]	Rise/Fall time	D* [Jones]	Bending cycle	Washing cycle	
SLG/PVK (Fibre) [THIS WORK]	2.2×10^4 @1 V 488 nm	480-870	9/33 ms	10^{13}	4 mm 100 cycles	AATCC 30 cycles	Flexible PDs
CuZnS/TiO$_2$ (Fibre)[31]	640 @3 V 320-400 nm	260-420	200/200 ms	–	60^0 200 cycles	–	
Carbon fibre/ZnO-CdS (Fibre)[34]	10^5 @2 V 372 nm	372-548	>1 s	–	-0.38%strain -	–	
P3HT/ZnO (Fibre)[39]	156μ @0 V 365 nm	365-880	40/40 ms	0.74×10^9	1.96% strain -	–	
Carbon fibre/PVK (Fibre)[35]	0.563 @0 V 800 nm	350-1050	200/200 ms	2.15×10^{13}	90^0 60 cycles	–	
PVK (PET)[127]	3.49 @3 V 365 nm	365-780	0.14/2.9 s	–	ND 120 cycles	–	
PVK/PDPP3T (PET)[140]	154×10^{-3} @1 V 835 nm	365-835	–	8.8×10^{10}	7 mm 1000 cycles	–	
SLG/MoS$_2$ (1L) (PET)[130]	45.5 @1 V 642 nm	–	–	–	14 mm 30 cycles	–	
InP (PET)[138]	0.12 @-0.3 V 533 nm	533-980	–	–	38.1 mm -	–	
SLG/PVK (PA)[139]	115 @1 V 515 nm	–	5.3 s	3×10^{12}	12 mm 3000 cycles	–	
SLG/CsPbBr$_3$ (Fibre(facet))[32]	2×10^4 @0.2 V 400 nm	400-520	24.2 s	8.6×10^{10}	NA	NA	Rigid PDs
MoS$_2$ (1L) (Fibre(facet))[33]	0.6 @4 V 400 nm	–	7.1/3.5 s	–	NA	NA	
PVK (Glass/ITO)[131]	27 @5 V 830 nm	400-830	30/20 μs	10^{13}	NA	NA	
SLG (Si/SiO$_2$)[124]	6.1×10^{-3} @0.4 V 1150 nm	300-6000	16 GHz	–	NA	NA	
SLG/PVK (Si/SiO$_2$)[117]	180 @0.1 V 520 nm	400-980	87/540 ms	10^9	NA	NA	
SLG/PVK (Si/SiO$_2$)[128]	10^9 @0.5V 598 nm	350-1100	4.5/57.5 s	10^{14}	NA	NA	
SLG/QDs (Si/SiO$_2$)[70]	10^7 @5 V 532 nm	532-1600	10/100 ms	7×10^{13}	NA	NA	
SLG/MoS$_2$ (Si/SiO$_2$)[129]	10^7 @1 V 532 nm	290-680	–	–	NA	NA	
Conductive microfluidized graphite-coated textile[40]	NA	NA	NA	NA	180^0 150 cycles	BS EN ISO 105 C06 A1S 10 cycles	Flexible Non PDs
Polymer solar cells[41]	NA	NA	NA	NA	52% compression 20 cycles	Submersed in water 20 cycles	
Textile-based field-effect transistors[74]	NA	NA	NA	NA	4mm-	Tumble-washed 20 cycles	

Fibres are an ideal platform for wearable electronics due to their deformability[6,21] and ease of integration into clothes.[6,21] They can be used to cover various geometries to make functional surfaces for wearable electronics.[22] To achieve this, fibre-based conductors, semiconductors, and insulators with controlled geometries and interfaces are required. These components could be used to integrate electronics into a textile during weaving,[15] for applications such as light-harvesting,[23,24] light-generation,[25] and photodetection.[26]

The integration of photodetectors (PDs) into clothes would enable features such as photoplethysmography[17] (i.e., analyzing the skin's optical absorption/reflectance to track changes in blood vessels' volume for cardiac pulse measurement),[27] and hazardous light detection (for skin cancer prevention).[31] A number of fibre-based PDs were reported for wearable applications.[28–35] These can be compared via a number of key performance indicators (KPIs) including (i) external responsivity:[36]

$$R_{ext} = \frac{\triangle I_{ph} h c}{q . P_{opt} . \lambda . A_{PD}/A_0} \tag{1}$$

where I_{ph} is the photocurrent, $I_{ph} = I_{light} - I_{dark}$, i.e., the difference between current under illumination and in dark, h is the Planck constant, c is the speed of light, q is the electron charge, P_{opt} is the impinging optical power, λ is the wavelength of the incident laser, A_{PD} and A_0 are the PD area and the laser spot size, respectively. A_{PD}/A_0 is a scaling factor taking into account that only a fraction of optical power impinges on the PD, (ii) response time (τ_{res}), i.e., the lifetime of the photogenerated charges in the PD light absorbing layer,[37] (iii) operating voltage,[37,38] (iv) R_{ext} or I_{ph} under mechanical distortion (e.g., bending),[26] and (v) washability, defined as the ability to withstand exposure to water and cleaning processes without being damaged or malfunctioning.[26]

State-of-the-art wearable fibre-based PDs have τ_{res} ∼40 ms[39] and R_{ext} ∼156 µAW^{-1}[39] at 365 nm. Under bending strain ∼1.96%, Ref. [39] reported that R_{ext} was enhanced ∼80% by the piezo-phototronic effect (i.e., three-way coupling of piezoelectric, semiconductor, and photonic properties)[39] compared to no strain. Refs. [40, 41] addressed washability in wearable e-textiles, but did not specifically focus on the washability of PD electronics. Ref. [40] reported microfluidized graphite (20% <10 nm thickness after 20 cycles of microfluidization) based poly-cotton fabric,[40] with a polyurethane-based encapsulant to fabricate graphene-coated textiles. They measured 3.5 times higher resistance (∼700 Ωcm^{-1}) after ten washing cycles.[40] Ref. [41] showed washable polymer solar cells made of donor-acceptor polymer with quaterthiophene and naphtho[1,2-c:5,6-c']bis[1,2,5]thiadiazole (NTz) (PNTz4T) and [6,6]-phenyl C$_{71}$-butyric acid methyl ester (PC$_{71}$BM). Ref. [41] demonstrated that flexible photovoltaic modules encapsulated with ∼1 µm parylene and ∼500 µm acrylic elastomers maintained ∼80% of the initial power conversion efficiency (i.e., the percentage of solar energy converted into usable electricity)[38] after water submersion for 100 min.[41] Ref. [33] prepared PDs on the end-face of an optical fibre using monolayer (1L) MoS$_2$ prepared by chemical vapor deposition (CVD). This was wet transferred and dip coated onto the fibre facet (end-face).[33] Ref. [33] reported R_{ext} ∼0.6 AW^{-1} at 4 V and 400 nm, with rise time and fall times (i.e., the time for

the signal to rise from 10% to 90%[38] or fall from 90% to 10% of the final value)[38] ∼7.1s and ∼3.5 s, respectively.[33] However, PD fabrication on fibres' facets is not practical for wearable applications, since fibres' facets can be covered and hindered during weaving,[42] thus not being able to receive light.[26] PDs built parallel to the longitudinal axis of fibres are desired,[26] so that the exposed portion receives light, and the covered conductive terminals transmit the signals. Ref. [34] prepared PDs made of ZnO-CdS double-shell nanowire arrays on carbon fibres,[34] with R_{ext} ∼10^5 AW^{-1} at 372 nm at 2 V, τ_{res} >1 s[34] with operating wavelength from 372 to 548 nm.[34] Ref. [35] reported fibre-shaped PDs based on CH$_3$NH$_3$PbI$_3$ perovskite(PVK)/TiO$_2$/carbon fibres and Cu wires, achieving τ_{res} ∼200 ms, with R_{ext} ∼1.48 AW^{-1} under 0.5 V at 800 nm and 0.563 AW^{-1} at a 0 V bias at 800 nm. Ref. [31] demonstrated fibre-shaped CuZnS/TiO$_2$ nanotubes PDs with Ti wires as inner electrodes and wrapped carbon nanotube around the wire as the outer electrode,[31] with R_{ext} ∼640 AW^{-1} under UV-A (320–400 nm) at 3 V, τ_{res} ∼200 ms and operating wavelength ∼260–420 nm, limited by the absorption of TiO$_2$ nanotubes.[31] Bending to 90° up to 60 cycles[35] and 60° for 200 cycles[31] resulted in ∼8% and ∼14% decrease of I_{ph}, respectively,[31] see **Table 1**. However, none of these reported washability tests, see Table 1 for a summary.

Graphene and related materials (GRMs) are ideal for a variety of optoelectronics applications,[44] such as PDs,[37] solar cells,[45–47] and modulators.[48,49] Wafer-scale growth, transfer and fabrication of CVD SLG have improved over the years,[50–52] with carrier mobility, µ, reaching ∼18500 $cm^2 V^{-1} s^{-1}$ at room temperature (RT) on a rigid substrate such as Si/SiO$_2$.[67] CVD SLG without encapsulation on ethylene vinyl acetate (EVA)/polyethylene terephthalate (PET) was reported with µ up to ∼7000 $cm^2 V^{-1} s^{-1}$.[53] However, the absence of a gain mechanism that can generate multiple charge carriers from one incident photon, resulted in limited R_{ext} ∼0.01 AW^{-1} for SLG-only PDs.[71]

PVKs are promising photoactive materials, due to their long(>1 µm)[54] charge-carrier diffusion lengths,[54] strong (∼10$^5 cm^{-1}$)[55] absorption coefficients,[55] and bandgap tunability (from 1.1 eV[56] to 2.5 eV[56]) via chemical composition control.[56] PVKs could be applied for coloured emitters,[57] energy harvesting,[58] and PDs.[59,60] PVKs based PDs have low R_{ext} ∼0.4 AW^{-1} in the UV-visible range (350–900 nm),[61,62] mainly due to low µ ∼40 $cm^2 V^{-1} s^{-1}$,[63] since R_{ext} is proportional to µ:[36]

$$R_{ext} = \frac{\Delta I}{P_{opt}} \frac{\tau_{life} \mu V_{ds}}{L^2} \tag{2}$$

where τ_{life} is the response time, V_{ds} is the bias applied between source and drain, and L is the channel length. The term $\frac{\tau_{life} \mu V_{ds}}{L^2}$ is called gain.[36] By increasing µ, the gain increases, which results in higher R_{ext}. Consequently, the combination of solution-processed PVK with SLG having µ well above that of PVK, to enhance gain, is promising for light sensing and flexible applications.

Ref. [32] prepared PDs based on SLG and CsPbBr$_3$ PVK nanocrystals at the end-face of silica fibres with R_{ext} ∼2 × 10^4 AW^{-1} under 400 nm illumination. SLG was transferred onto the facet, followed by self-assembly of CsPbBr$_3$ nanocrystals.[32] However, the operating wavelength was ∼400–520 nm, limited

**ADVANCED
SCIENCE NEWS**

www.advancedsciencenews.com

**ADVANCED
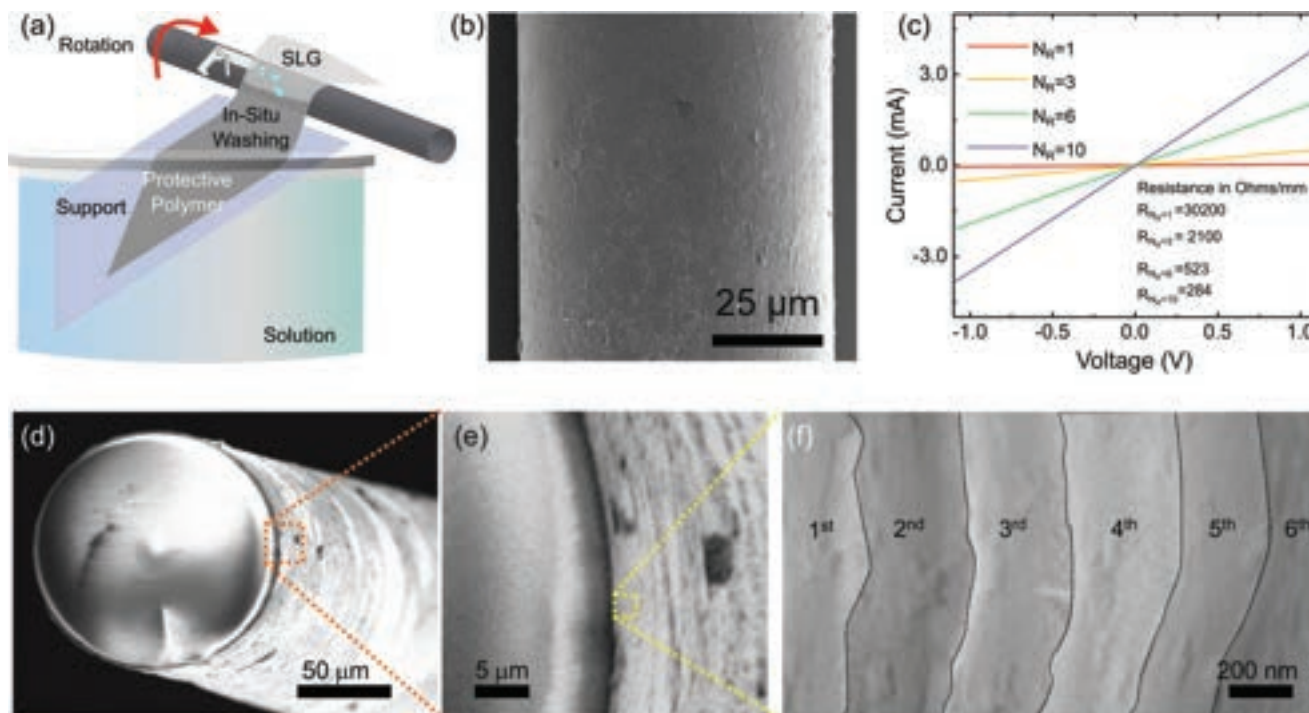MATERIALS**

www.advmat.de

Figure 1. a) Scheme of transfer process for CVD SLG around fibres. b) Top view SEM images for $N_R = 6$. c) Current vs voltage of fibres as a function of N_R. d) Cross-section SEM image for $N_R = 6$. e) Zoom-in of dashed square in d) shows cross-sectional multi-layer coating of SLG on fibre. f) Zoom-in of dashed square in (e) shows multi-layer coating of SLG with residual PMMA layers. The image is contrast-edited for each layer, dashed lines indicate the presence of SLG, and numbers indicate the rolling layer.

by the $CsPbBr_3$ nanocrystals absorptions,[32] with τ_{res} ~24.2 s, Table 1.

Here, we report a wet transfer approach to roll CVD SLG around silica fibres, to be used as a gate for flexible PDs. This is followed by the deposition of Al_2O_3 and parylene C as dielectrics. Another rolled SLG is used as channel with μ ~1300 $cm^2 V^{-1} s^{-1}$ at RT, before depositing $(Cs_{0.06}FA_{0.79}MA_{0.15})Pb(I_{0.85}Br_{0.15})_3$, where MA = methylammonium, CH_3NH^{3+} and FA = formamidinium, $CH_3(NH_2)^{2+}$ PVK as photoactive layer. Our PVK does not degrade up to 85 °C[72] and is chemically stable (ions do not migrate to other layers (i.e., SLG)).[73] We get R_{ext} ~22,000 AW^{-1} at 488 nm, with rise and fall times ~9 and ~33 ms, respectively, at 1 V, outperforming R_{ext} of fibre-based PDs by at least two orders of magnitude[31,33,35] and one order of magnitude in τ_{res},[31,32,35] Table 1. Bending and washing tests are also performed. After 100 bending cycles at a 4 mm bending radius I_{ph} is ~80% of the non-bent one. After 20 and 30 washing cycles according to the AATCC standard[9] we get ~6% and ~28% degradation of I_{ph}. The washability of our fibre-based PDs goes beyond the typical 20 cycles reported in the literature for textile-based field-effect transistors (FETs).[74] Ref. [74] reported ~50% drop in drain current after 20 washing cycles, while our PDs maintain up to ~72% of the I_{ph} after 30 cycles, making them promising for wearable applications.

2. Results and Discussion

Figure 1a plots a scheme of the transfer process of CVD SLG around fibres. To transfer SLG, poly(methyl methacrylate)

(PMMA) dissolved in acetone is spin-coated on SLG/Cu at 4000 rpm for 40 s, followed by oxygen etching of SLG on the Cu backside using an RIE-NanoEtch (3 W, 30 s).[75,76] Cu/SLG/PMMA is then transferred to an aqueous ammonium persulfate (APS) solution $((NH_4)_2S_2O_8,$ 0.5 molL^{-1}) for Cu dissolution.[75,76] The PMMA membrane and CVD SLG are then cleaned of APS residuals by dipping in DI water for 20 min. This is followed by the rolling process. First, the fibre is placed on a supporting film (e.g., PET) and the edge of the floating SLG/PMMA is fished onto the fibre, while the rest of the SLG/PMMA stays on the supporting film. Then, the fibre is rotated clockwise at ~10 rpm to roll SLG/PMMA. The PMMA layer is then removed by immersing the coated fibre in acetone for 15 min, followed by rinsing with isopropanol for 10 min and drying in N_2. Figure 1b is the top view of 6 SLG layers coated on fibre glass, taken by scanning electron microscopy (SEM, Magellan 400 L).

Figure 1c plots the current (measured via a Keithley source meter at the two ends of the channel layer) of coated fibres with different number of rolled SLG, N_R, for a channel length ~1 mm. The linear relation between current and voltage indicates Ohmic conductivity.

Figure 1d shows the cross-section SEM image for fibre-based PDs with $N_R = 6$. Figure 1e is a close-up of the dashed square in Figure 1d, revealing a cross-sectional multi-layer coating of SLG on the fibre. Figure 1f is a zoom in of the dashed square in Figure 1e, illustrating the multi-layer coating of SLG along with residual PMMA layers.

Given that increasing N_R reduces sheet resistance[45] due to increased conductive paths,[77] $N_R = 6$ is chosen as a gate electrode.

**ADVANCED
SCIENCE NEWS**

www.advancedsciencenews.com

**ADVANCED
MATERIALS**

www.advmat.de

$N_R = 10$ leads to 284 Ωmm^{-1}, however the roughness caused by PMMA residuals between the layers could result in a short circuit in the PDs when the dielectric layer is positioned between gate and channel layer. Thus, we use $N_R = 6$ to fabricate conductive fibres with a uniform surface coverage of SLG as for Figures 1b,d.

The presence and quality of SLG are further studied by Raman spectroscopy. **Figure 2** plots the Raman spectrum of SLG as-grown on Cu. The 2D peak is a single Lorentzian with Full Width at Half Maximum, FWHM(2D) ~34 cm^{-1}, signature of SLG.[79] The position of the G peak, Pos(G), is ~1591 cm^{-1}, with FWHM(G) ~22 cm^{-1}. The 2D peak position, Pos(2D), is ~2720 cm^{-1}, with FWHM(2D) ~34 cm^{-1}, while the 2D to G peak intensity and area ratios, I(2D)/I(G) and A(2D)/A(G), are ~4.4 and ~6.7. No D peak is observed, indicating negligible defects.[80] Figure 2 plots Raman spectra of CVD SLG for $N_R = 1$, 2, 4, 6, 8, 10. The 2D line shape is independent of N_R, suggesting no interaction between the transferred SLGs,[80,81] Figure 2.

Figure 3 plots Pos(G), FWHM(G), Pos(2D), FWHM(2D), I(2D)/I(G), A(2D)/A(G), I(D)/I(G) as a function of N_R. For each N_R, ten points are collected along the fibre. I(2D)/I(G) changes from ~2.4 for $N_R = 1$ to ~1.7 for $N_R = 10$, Figure 3a. A(2D)/A(G) changes from ~4.0 for $N_R = 1$ to ~2.9 for $N_R = 10$, Figure 3b. The decrease in I(2D)/I(G) and A(2D)/A(G) indicates doping increases from E_F ~225 meV for $N_R = 1$ to ~320 meV for $N_R = 10$.[82,83] This is further supported by the decrease of Pos(G) as function of N_R from ~1585.4 cm^{-1} for $N_R = 1$ to 1584.3 cm^{-1} for $N_R = 10$, Figure 3d. From I(D)/I(G), Figure 3g, the defect density changes from ~5.74 × 10^{10} cm^{-2} for $N_R = 1$ to ~7.1 × 10^{10} cm^{-2} for $N_R = 10$[84,85] for excitation energy 2.41 eV and E_F ~225 meV and 320 meV, respectively, Figure 3g. FWHM(2D,G) are broadened as N_R increases due to defects and inhomogeneities of rolled CVD graphene, Figures 3c,e.

For $N_R = 6$, Pos(G) ~1584 cm^{-1}, FWHM(G) ~21 cm^{-1}, Pos(2D) ~2694 cm^{-1}, FWHM(2D) ~38 cm^{-1}, I(2D)/I(G) ~1.7 A(2D)/A(G) ~2.9, indicating p doping with E_F ~310 meV by taking into account the dielectric constant ~3.9 of the silica fibre.[86] I(D)/I(G) ~0.10 corresponds to a defect density ~4.9 × 10^{10} cm^{-2}.[84,85] Pos(G) and Pos(2D) are affected by the presence of strain. Biaxial strain can be differentiated from uniaxial from the absence of G-

peak splitting with increasing strain,[87] however at low (≲0.5%) strain the splitting cannot be resolved.[87,88] For uniaxial(biaxial) strain, Pos(G) shifts by ΔPos(G)/Δε$_{strain}$ ~F23(60) cm^{-1}/%.[87,88] Pos(G) also depends on doping.[82,83] However, Pos(2D) and Pos(G) are not correlated, Figure 3h. Thus, the spread of Pos(G) and Pos(2D) is mostly due to doping. **Table 2** summarizes the Raman fit parameters and the resulting Fermi energy, E_F, doping type (n or p), strain, and defect density.

Figure 4 is a schematic drawing of our fibre-based PDs. The fabrication process starts by wiping the silica fibre via acetone and isopropanol, Figure 4a. CVD SLG is rolled 6 times around the fibre (reaching a conductivity ~500 Ωmm^{-1} to form a gate electrode, Figure 4b). Then, 150 nm Al$_2$O$_3$ and 200 nm parylene C are deposited as gate-dielectrics, Figure 4c. Al$_2$O$_3$ is commonly used as a gate dielectric in graphene FET[89] because of its dielectric constant ($k ≈ 9$),[90,91] compatibility with graphene[91] and breakdown voltage (up to 10 MVcm^{-1}).[90] Parylene is also commonly employed as dielectric, pin-hole free,[92,93] passivation layer[94] in flexible electronics.[95,96] Al$_2$O$_3$ coating is performed by atomic layer deposition (ALD, Cambridge Nanotech Savannah), to achieve uniform coating and film thickness control (down to the nm range).[97] We deposit a 150 nm-thick Al$_2$O$_3$ dielectric layer at 150 °C at a base pressure ~0.5 mbar using trimethyla-luminum (TMA purity >98%, Strem Chemicals 93–1360) as a precursor and H$_2$O as oxidant. Oxidant and precursors are alternately introduced into the chamber in a 20 sccm flow of N$_2$ carrier gas. If Al$_2$O$_3$ alone is used, we get dielectric failure because of crack formation, due to the mechanical stress/strain involved in the fabrication process of our PDs. 200 nm parylene is applied as follows. A parylene dimer is vaporized at 80 °C, then, in a separate chamber, it is pyrolyzed into monomers at 690 °C. The fibre is held at RT, so that the parylene polymerizes on contact with the surface. The physical vapor deposition of parylene provides coverage of all accessible surfaces.[98] This improves the dielectric robustness against deformations during the manufacturing of fibre-based PDs, reducing the risk of short circuits. The sole use of parylene C, however, creates inconsistent dielectric properties: thin layers (~500 nm) result in gate leakage at low (~0.2 MVm^{-1}) electric fields while exceeding 500 nm compromises the channel modulation due to a decrease in the gate dielectric capacitance.[99] Another $N_R = 6$ CVD SLG is then rolled as channel material, Figure 4d.

Figure 5 plots the Raman spectra of the fibre PD at different fabrication stages. Since the device fabrication comprises many steps, monitoring the graphene quality is essential, as it could affect μ, thus R$_{ext}$, Equation (2). Figure 5c shows the Raman spectra of fibre (red), dielectric layer (150 nm Al$_2$O$_3$ and 200 nm parylene C) (blue), $N_R = 6$ on the dielectric layer (green), and coated PVK on $N_R = 6$ (orange). In the Raman spectrum of Al$_2$O$_3$ and parylene C, the peaks ~1337, 1440, and 1610 cm^{-1}, Figure 5c, are attributed to CH$_2$ wagging and twisting vibrations,[100,101] CH scissoring in CH$_2$ and/or C-C skeletal in-plane vibrations of the aromatic ring,[100,101] and CH scissoring in CH$_2$ and/or C-C skeletal in-plane vibrations of the aromatic ring,[100,101] respectively. For $N_R = 6$, Pos(G) ~1587 cm^{-1}, FWHM(G) ~17 cm^{-1}, Pos(2D) ~2686 cm^{-1}, FWHM(2D) ~41 cm^{-1}, I(2D)/I(G) ~1.9 and A(2D)/A(G) ~4.7. Pos(2D) ~2686 cm^{-1} indicates that layers are p-doped.[83] From A(2D)/A(G) ~4.7 we estimate E_F ~190 meV, corresponding to a carrier concentration ~2.2 × 10^{12} cm^{-2} by taking
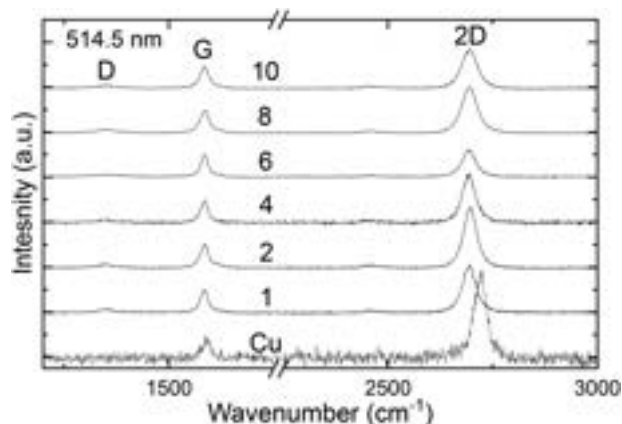
Figure 2. 514.5 nm Raman spectra of CVD SLG on Cu and for $N_R = 1$, 2, 4, 6, 8, 10, normalized to have the same I(G). At least ten points are collected along the fibre.

Figure 3. 514.5 nm Raman spectra for $N_R = 1, 2, 4, 6, 8, 10$. For each N_R, ten points are collected along the fibre. a–g) Average and standard deviations of a) I(2D)/I(G), b) A(2D)/A(G), c) FWHM(G), d) Pos(G), e) FWHM(2D), f) Pos(2D), g) I(D)/I(G). h) Pos(2D) as a function of Pos(G).

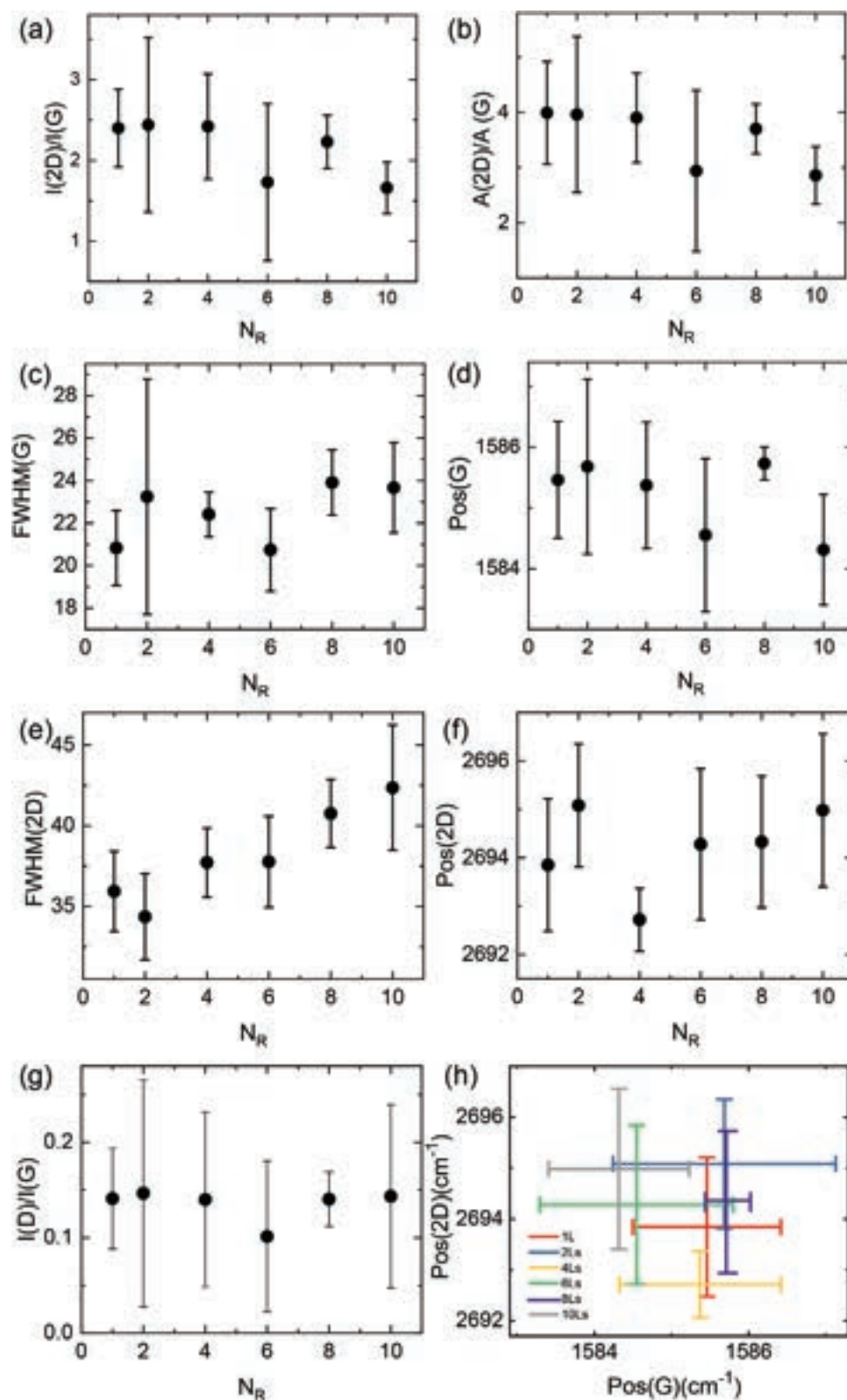**Table 2.** The Raman fit parameters, resulting E_F, doping type (n or p), strain, and defect density. The first row relates to rolled SLG on the fibre (gate), while the last two rows correspond to a fibre with a dielectric layer (150 nm Al_2O_3 and 200 nm parylene C) (channel). For each sample, at least five points are collected, and the mean with standard deviation (±) given.

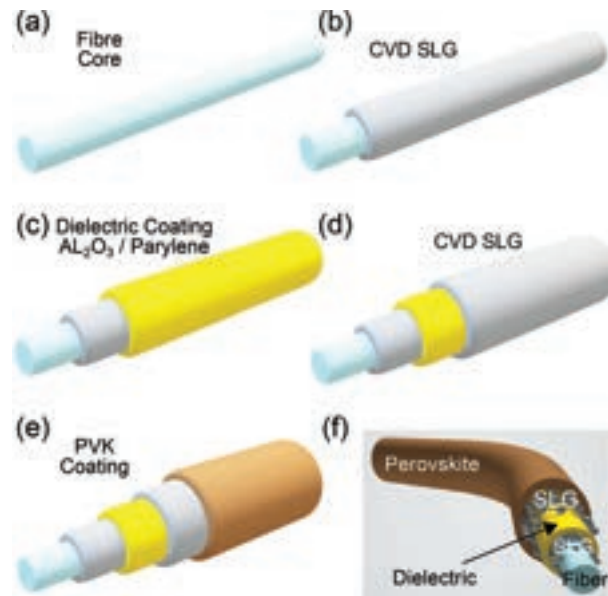| Sample	Pos(G) cm⁻¹	FWHM(G) cm⁻¹	Pos(2D) cm⁻¹	FWHM(2D) cm⁻¹	A(2D)/A(G)	I(2D)/I(G)	I(D)/I(G)	E_F meV	Doping type	Uniaxial strain% Biaxial strain%	defect density × 10^{11} cm⁻²
N_R = 6	1584 ±1	21 ±2	2694 ±2	38 ±3	2.9 ±1.5	1.7 ±0.9	0.10 ±0.08	310 ±110	p	0.40 ±0.04 0.15 ±0.02	0.49 ±0.12
N_R = 6	1587 ±1	17 ±2	2686 ±3	41 ±3	4.7 ±1	1.9 ±0.3	0.49 ±0.1	190 ±20	p	-0.06 ±0.06 -0.02 ±0.02	1.82 ±0.39
N_R = 6/PVK	1583 ±1	17 ±2	2701 ±3	43 ±3	2.3 ±0.6	0.9 ±0.3	0.46 ±0.1	380 ±30	p	0.60 ±0.03 0.20 ±0.01	2.48 ±0.62

Figure 4. Fibre-based SLG/PVK PDs fabrication process. a) Silica fibre substrate. b) N_R = 6 around the fibre as a gate electrode. c) Gate dielectric layer composed of Al_2O_3 and parylene C. d) Rolled N_R = 6 channel. e) Spin-coated PVK on rolled CVD SLG channel. f) Assembled fibre-based SLG/PVK PD.

into account the dielectric constant ∼3[102] of Parylene and residual PMMA from transfer of CVD SLG.[83] I(D)/I(G) ∼0.49 corresponds to a defect density ∼1.82 × 10¹¹ cm⁻²[84,85] for 2.41 eV and E_F ∼190 meV. The Fermi level, E_F, from A(2D)/A(G) should correspond to Pos(G) ∼1586 cm⁻¹ for unstrained graphene.[82] However, in our experiment Pos(G) ∼1587 cm⁻¹, which implies a contribution from compressive uniaxial (biaxial) strain ∼0.06% (0.02%).[87] Table 2 summarizes the Raman fit parameters and the resulting E_F, doping type (n or p), strain, and defect density.

Source and drain electrodes are defined (channel length: 1000 μm; diameter: 125 μm) by inkjet printing Ag ink (Sigma–Aldrich, 736465) (resistivity = 11 μΩcm). Ag ink is also printed on the gate, and the ink is cured on a hot plate at 150 °C for 1h to remove the residual solvent (triethylene glycol monomethyl ether). We use a Fujifilm Dimatix DMP-2800 with a 21 μm diameter nozzle. This approach removes the need for conventional lithography,[103] or shadow masks.[104]

Then, a mixed-cation lead mixed-halide PVK[63] is prepared as discussed in methods. The PVK solution is spin-coated (Figure 4e) on the surface-treated rolled SLG surface (10 min under UV-Ozone Cleaner UVC-1014, to facilitate the dispersion of PVK, by making the surface hydrophilic)[105] using a two-step speed program at 2000 and 6000 rpm for 10 and 30 s, respectively, adding 150 μl of chlorobenzene 30 s after the start of the spinning routine.[106] These different speeds allow us to get more homogeneity with respect to one-step spinning,[106] and remove solvents during the PVK film formation.[106] The samples are annealed at 100 °C for 1 h to remove the solvents (Dimethylformamide and Dimethyl sulfoxide).[106] All processes to make and spin coat PVK are performed in a N_2-filled glove box to prevent degradation of PVK triggered by H_2O.[107] To prevent PVK
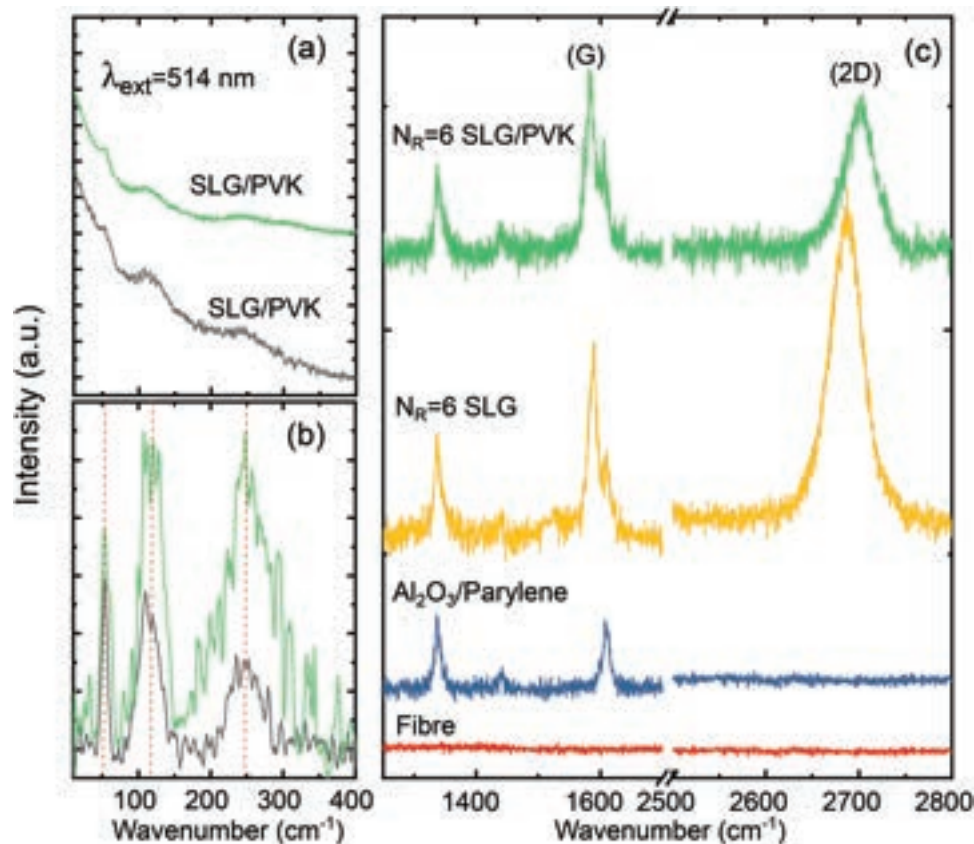
Figure 5. a) Raman spectra of SLG/PVK on fibre (green) and SLG/PVK on Si/SiO₂ (gray). b) Backgrounds subtracted spectra from (a). c) Raman spectra of fibre (red), fibre/dielectric (Al₂O₃ and parylene) (blue), fibre/dielectric/N$_R$ = 6 (orange), fibre/dielectric/N$_R$ = 6/PVK (green). The PL background of PVK is subtracted for the green spectrum. All measurements taken at 514.5 nm. For each spectrum, at least five points are collected.

oxidation and degradation during electrical and photodetection characterizations, the SLG/PVK PD is sealed under vacuum using Parylene C dimers (Curtiss-Wright) with a Parylene coater (SCS coating). This forms a barrier to moisture and gas permeability.[108,109] Following encapsulation, our SLG/PVK PDs are stable for > 30 days under ambient conditions.

Figure 5a plots the Raman spectra of SLG/PVK on fibre (green) and Si/SiO₂ (gray) for 514.5 nm excitation. These show three bands ~52, 110, 249 cm^{-1}. The PL background of PVK can be seen in Figure 5a and background subtracted spectra are in Figure 5b. The bands ~52 and 110 cm^{-1} are the main modes of PVK[110] assigned to PbBr₆ deformation[111,112] and motion of the organic cation,[111,112] respectively. The peak ~249 cm^{-1} is assigned to torsional mode of the methylammonium cation, due to PVK exposure to moisture.[110,113] Moisture could be introduced when the sample is removed from the glove-box, prior to sealing with parylene. After the deposition of PVK on N$_R$ = 6, Figure 4e, the Raman spectrum of N$_R$ = 6 has Pos(G) ~1583 cm⁻¹, FWHM(G) ~17 cm⁻¹, Pos(2D) ~2701 cm⁻¹, FWHM(2D) ~43 cm⁻¹, I(2D)/I(G) ~0.9 and A(2D)/A(G) ~2.3. Pos(2D) ~2701 cm⁻¹ indicates p-doping.[83] From A(2D)/A(G) ~2.3 we estimate E$_F$ ~380 meV, which corresponds to a carrier concentration ~8.8 × 10¹² cm⁻², by taking into account the dielectric constant of Parylene and residual PMMA.[83] I(D)/I(G) ~0.46 corresponds to a defect density

~2.48 × 10¹¹ cm⁻²[84,85] for 2.41 eV excitation and E$_F$ ≈~380 meV. E$_F$ as estimated from A(2D)/A(G) should correspond to Pos(G) ~1596 cm⁻¹ for unstrained graphene.[82] However, in our experiment Pos(G) ~1583 cm⁻¹, which implies tensile uniaxial (biaxial) strain ~0.6%(0.2%).[87]

Figure 6a is an SEM image of the spin-coated PVK on N$_R$ = 6. This shows uniform coverage. An average roughness ~20 nm is measured with a Bruker Dimension Icon atomic force microscope (AFM) in Figure 6b. Figures 6c-e are optical images of the final device.

Figure 7a plots the absorbance from photo-thermal deflection spectroscopy (PDS) of individual SLG and PVK films on quartz, compared with SLG/PVK. PDS can measure the band-tails of PVK down to ~10⁻⁵ absorbance.[114] Figure 7a shows that PVK absorption increases for SLG/PVK compared to PVK. This indicates the presence of interface states that alter the PVK bandgap.[114] The PL spectra of PVK and SLG/PVK are in Figure 7b. Both show a PL peak ~762 nm arising from the PVK band gap.[63] The PL intensity (integrated area under PL curve) of SLG/PVK is quenched ~96% compared to PVK. This can be assigned to charge carrier transfer between PVK and SLG,[115] though there is also increased non-radiative recombination due to the increased sub-gap trap density, as shown by the PDS measurements in Figure 7a.
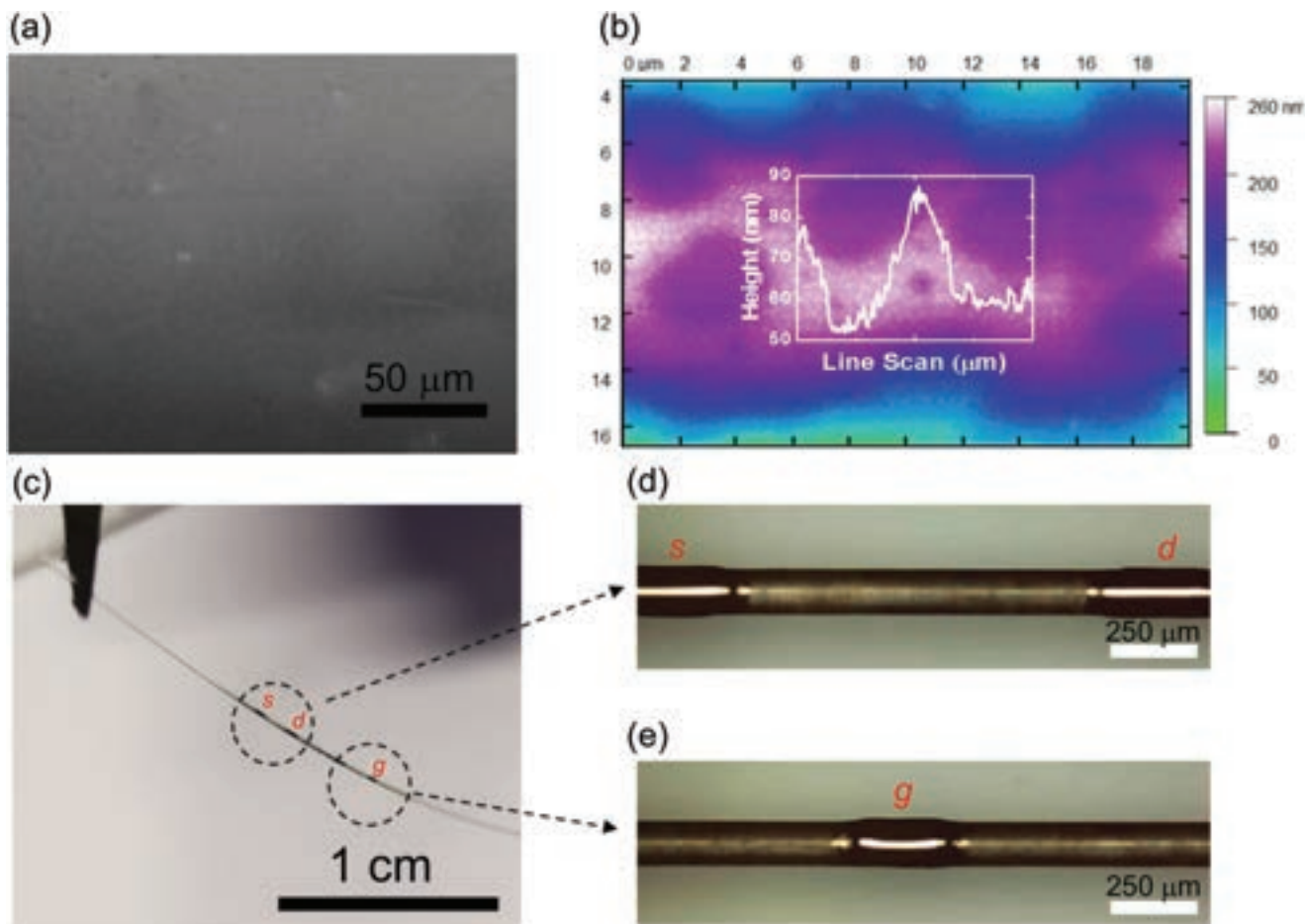
Figure 6. a) SEM and b) AFM image of PVK film on N_R = 6. Inset shows the roughness of spin-coated PVK film. c–e) Optical microscopy images of final device. d,e) Source-drain and gate electrodes are printed using Ag ink. s, d, g: source, drain, gate.

Time-resolved PL (TRPL) spectra are recorded at RT to study charge transfer at the SLG/PVK interface. We fit Figure 7c to calculate average lifetimes to compare the amount of charge quenching, but we do not imply any physical meaning to this fit. We use the relation:[38]

$$f(t) = \sum_i A_i exp(-t/\tau_i) + B \qquad (3)$$

where A_i is decay amplitude, τ_i is decay time and B is constant. The PL decay times for PVK are τ_1 = 6.7 ns (A_1:0.802) and τ_2 = 32.9 ns (A_2:0.198), with average lifetime $(\Sigma A_i \tau_i)/(\Sigma A_i)$ ∼11.8 ns. The PL decay times for SLG/PVK are τ_1 = 2.0 ns (A_1:0.743) and τ_2 = 10.7 ns (A_2:0.257), with average lifetime ∼4.3 ns, indicating charge transfer between SLG and PVK,[116] because of band energy alignment at the PVK/SLG interface.

We then characterize the photoresponse of the fibre-based PDs. The linear dependence of current versus voltage in **Figure 8a** indicates Ohmic contact of CVD SLG and Ag electrodes. By depositing PVK, the current increases in Figures 8a,b, suggesting h transfer from PVK to SLG, as shown in the band energy alignment at the PVK/SLG interface in Figure 8a. This is in agreement with PL quenching and shortening in the average lifetime (Figure 7b,c). Raman measurements in Figure 5 confirm an increase in the doping level of p-type SLG by adding PVK. A similar h transfer was previously reported for SLG/PVK interfaces.[117,118] To evaluate the influence of the PVK layer thickness, 3 thicknesses (93, 211, 626 nm) of coated PVK layers on SLG are prepared, Figure 8b. For the fibre-based PDs with 93 nm thickness, we measure 81 µA at 1 V, for 211 nm, we get 142 µA at 1 V. Thus, by increasing thickness, I_{ph} increases, suggesting stronger absorption and more generation of excitons and h transfer to SLG. At ∼3626 nm, I_{ph} decreases (122µA at 1V) as most photons are absorbed by the outermost layer, resulting in fewer photons reaching the underlying layers and, consequently, less I_{ph}. A thicker layer results in more scattering and recombination of excitons, further decreasing the I_{ph}. Therefore, we set the thickness at 211 nm.

The field-effect µ is calculated as:[36]

$$\mu = \frac{\triangle I_d . L}{\triangle V_g . C_{ox} . V_{ds} . 2\pi r} \qquad (4)$$

The field-effect µ for SLG is ∼1300 $cm^2 V^{-1} s^{-1}$ at RT, whereas for N_R = 6 it is ∼1100 $cm^2 V^{-1} s^{-1}$. This may be due to increased polymer residuals or defects, typically leading to diminished SLG
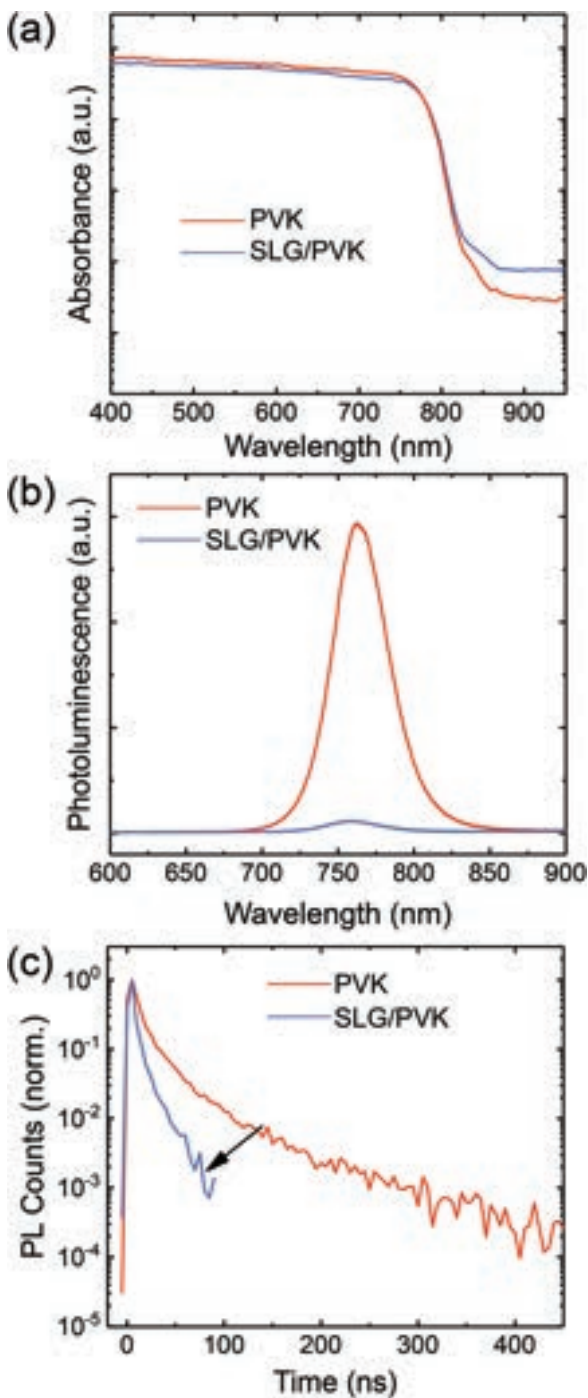
Figure 7. a) Absorbance of PVK and SLG/PVK. b) PL of PVK and SLG/PVK for 514.5 nm excitation. c) TRPL spectra of PVK and SLG/PVK for 400 nm excitation. The arrow indicates a shorter lifetime.

quality by enhancing carrier scattering, thereby resulting in lower μ.[120] R_{ext} is directly proportional to $\sim\mu$, as for Equation (2), therefore rolled SLG with $\mu \sim 1300$ $cm^2 V^{-1} s^{-1}$ can enhance R_{ext} more than metals such as Au and Ag, which typically have $\mu \sim 30$–50 $cm^2 V^{-1} s^{-1}$ at RT.[38]

Figure 8c plots I_{ds} versus V_g when the PD is illuminated at 488 nm for normal incidence with a collimated laser (Multi-Channel Source-Thorlabs) with P = 44 μW to 2 nW for V_{ds} = 0.5 V. We use a three-terminal device to explore the gate-dependent I_{ph}. This configuration can boost I_{ph} and elevate R_{ext}.[117,118] By modulating the SLG E_F via gating and utilizing a photogating effect, the built-in field at the SLG/PVK interface can be enhanced, potentially resulting in further charge transfer from PVK to SLG.[117,118] Under illumination, light is absorbed by PVK and part of the photogenerated h is transferred from the PVK valence band into the lower energy states in p-doped SLG,[117,118] leaving behind the uncompensated charge of photogenerated e.[117,118] The latter are trapped in PVK and act as an additional negative gate voltage, applied to the SLG channel, altering the electric field at the SLG/PVK junction.[117,118] -2<V_g <+10 is used as a safe range to avoid dielectric breakdown. The gate-source current is kept <1 nA to avoid leakage. A gate-dependent I_{ph} is not observed in our channel, Figure 8c. Due to the ultrafast (sub-100 fs) charge recombination in SLG,[121] the photogenerated carriers do not contribute to I_{ph}. The photocurrent is defined as:[36]

$$\triangle I_{ph} = I_{light} - I_{dark} \tag{5}$$

where I_{light} is the output current of the device under the incident beam, and I_{dark} is the current measured in dark. The photocurrent of the fibre-based SLG/PVK PDs is in Figure 8d, for P ranging from 980 μW to 750 pW, and V_{ds} from -1 to 1V. The corresponding R_{ext} as a function of power density is in Figure 8e. To calculate the exposed area, we consider only the curved surface area (πrL), assuming light exposure to half of the curved surface area. For A_{PD} and A_0 ~0.18 μm^2 and 0.78 5μm^2, respectively, we get R_{ext} ~22,000 AW^{-1} for P = 750 pW and V_{ds} = 1 V. For V_{ds} >1, the free carriers drift velocity, v_d, in SLG increases lineally until saturation by scattering with optical phonons.[123] Therefore, all measurements are done at $V_{ds} \leqslant$1V to keep the device operation in the linear (Ohmic) regime. A P rise leads to higher I_{ph} until saturation (44 and 980 μW), due to the increased recombination rate of photo excited carriers.[118] This R_{ext} is 7 orders of magnitude higher than the ~mAW^{-1} reported for SLG on flat and rigid substrates (e.g., Si/SiO$_2$,[71,124–126] one order of magnitude higher than reported for PVK on Si/SiO$_2$,[60] and 4 orders of magnitudes higher than pristine PVK ~3 AW^{-1}[127] on flexible PET substrates. Our R_{ext} is 2 orders of magnitude higher than PVK/SLG hybrid PDs on Si/SiO$_2$[117], but lower than the highest R_{ext} ~10^9 AW^{-1} PDs based on PVK/organic-semiconductor(poly-(3,4-ethylenedioxythiophene):poly(styrenesulfonate))[128] and lower than hybrid SLG/QDs[70] and SLG/MoS$_2$ PDs,[129] both with R_{ext} ~10^7 AW^{-1} on Si/SiO$_2$, see Table 1. However, our R_{ext} is the highest to date for fibre-based PDs in wearable applications, Table 1.

The temporal I_{ph} response is measured in Figure 8f via digital oscilloscope (MSO9404A). We use bi-exponential functions to fit the rise and decay times: $I(t) = I_{dark} + I_0[1 - exp^{(-t/\tau_{rise})}]$ and $I(t) = I_{dark} + I_0[exp^{(-t/\tau_{decay})}]$, with I_0 the maximum current at a particular time, τ_{rise} the rise time constant, τ_{decay} the decay time constant, and t the time for ON or OFF states duration. We get τ_1 = 4 ms (I$_1$:98.2) and τ_2 = 15 ms (I$_2$:72.8) with average rise time $(I_1.\tau_1+I_2.\tau_2)/(I_1+I_2)$ ~9 ms. The photoresponse decay times are τ_1 = 5 ms (I$_1$:41.6) and τ_2 = 43 ms (I$_2$:109.3) with average decay time ~33ms. The temporal τ_{res} of our fibre-based PDs is

**ADVANCED
SCIENCE NEWS**

www.advancedsciencenews.com
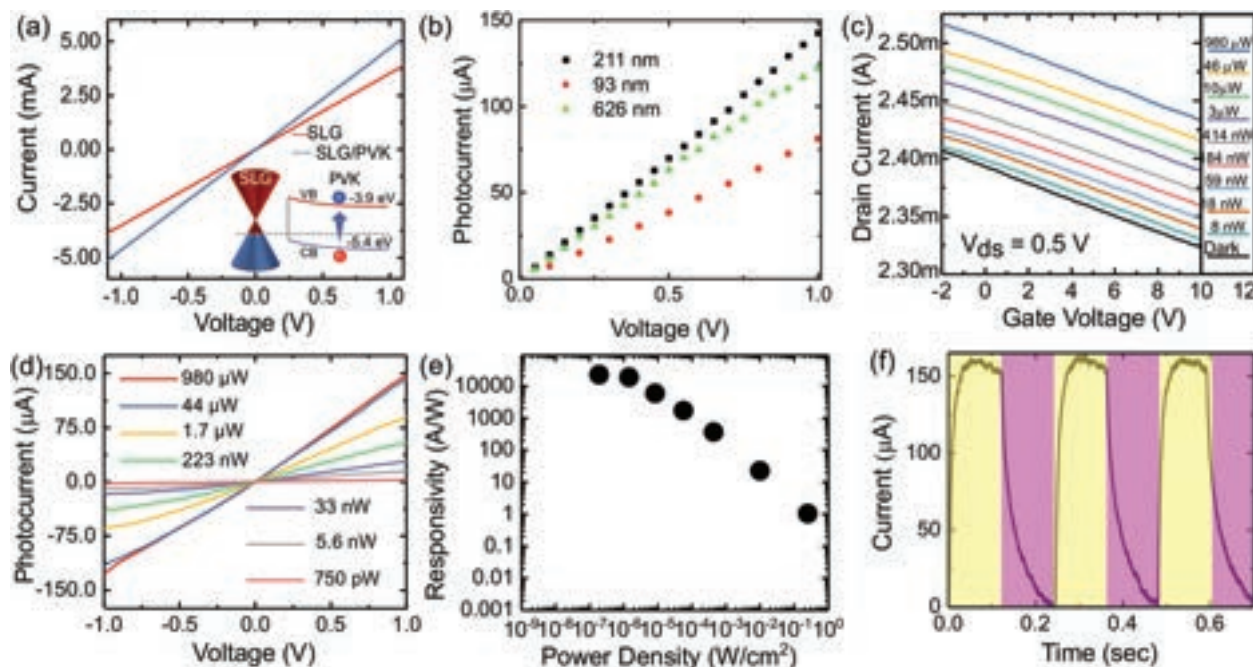
**ADVANCED
MATERIALS**

www.advmat.de

Figure 8. a) I_{ds} as a function of V_{ds} in dark before (red) and after (blue) deposition of PVK on $N_R = 6$. b) Variation of I_{ph} as a function of V_{ds} for 3 thicknesses (93, 211, 626 nm) of coated PVK layers on $N_R = 6$. c) Illumination power-dependent transfer characteristics at 488 nm. d) I_{ph} as a function of bias for different illumination powers and $V_g = 0$. e) R_{ext} as a function of optical power density. f) Temporal I_{ph} response for $N_R = 6$ under alternating dark (purple) and light (yellow).

faster than the ~200ms reported for carbon fibre/PVK PDs[35] and ~40ms for fibre-based P3HT/ZnO PDs,[39] and comparable to PDs made of exfoliated SLG and QDs on Si/SiO$_2$.[70]

The specific detectivity (D*) (($cm.Hz^{1/2}/W$) or Jones) relates the performance of PDs in terms of R_{ext} to the PD photoactive area, allowing the comparison of PDs with different active areas:[36]

$$D^* = \frac{(AB)^{1/2}}{NEP} \tag{6}$$

where A is the photoactive area (projected incident light on fibre), B is the electrical bandwidth (Hz) and NEP($W/Hz^{1/2}$) is the noise equivalent power (the power that gives a signal-to-noise ratio of 1 in a 1Hz output bandwidth) defined as:[132]

$$NEP = \frac{i_n}{R_{ext}} \tag{7}$$

where i_n is the dark noise current. The fibre PD is DC-biased with a source meter (Keithley 2612B). A chopper is used in the path of the incident beam to modulate the light.[132] The noise (A/$\sqrt{Hz}$) is characterized in the time domain collecting the trace on a digital oscilloscope, with subsequent Fourier transform to analyze the data in the spectral domain.

Figure 9a plots the spectral noise density as a function of frequency f. The measured noise in the dark shows a $1/f$ dependence. Thus, the noise density (i.e. noise power per unit of bandwidth (dbm.Hz$^{-1/2}$))[36] is inversely proportional to f, due to charge traps and defects.[36] Considering the measurement at 4Hz,~10 times less than the cut off f, defined as the f at which
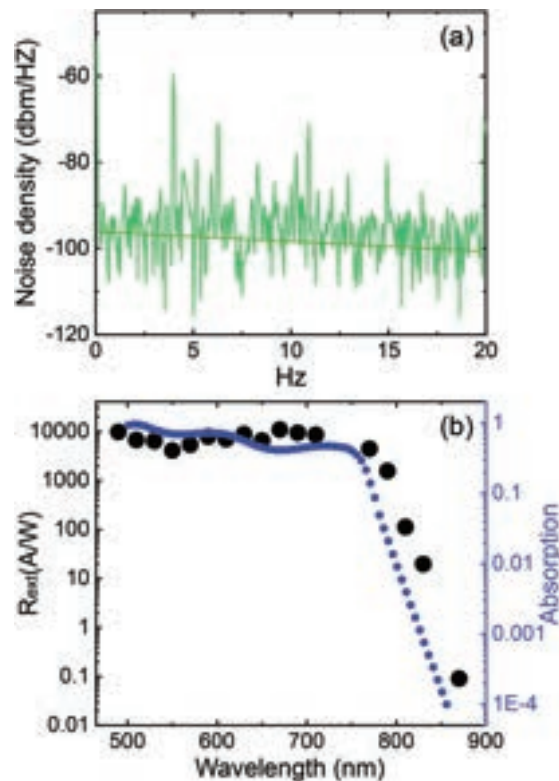

Figure 9. a) Spectral noise power of fibre PDs. b) Wavelength dependent R_{ext} for PDs and absorption of fibre PDs from the KK relations as a function of excitation wavelength.

**ADVANCED
SCIENCE NEWS**

www.advancedsciencenews.com

**ADVANCED
MATERIALS**

www.advmat.de

the detector R_{ext} decreases by 3dB,[36] we get NEP ~2.1×10^{-11} WHz$^{-1/2}$, D* ~2×10^9 Jones for N_R = 6. The noise current in the shot noise limit (due to generation and recombination of e-h pairs and resistive current paths in PDs[6]), can be expressed as $i_n = (2qI_{dark})^{1/2}$,[132,133] where the combined dark current (I_{dark}) is the sum of unamplified graphene current ($I_{dark(SLG)}$) and amplified injection current ($I_{dark(PVK)}$) from PVK, caused by the thermal excitations of charge carriers in the dark. $I_{dark(PVK)}$, due to thermal excitations of charge carriers in the dark, is much smaller than $I_{dark(SLG)}$ ~3.75 mA. Therefore, following Ref. [133], the shot noise limited noise current can be expressed as $i_n = (2qI_{dark(SLG)})^{1/2}$. D* in the shot noise limit can be written as:[132]

$$D^* = \frac{R_{ext}(AB)^{1/2}}{i_n} \qquad (8)$$

We get D* ~10^{13} Jones for N_R = 6. Our D* is comparable with that of state-of-the-art fiber based PDs,[35] where D* ~2.15×10^{13} Jones, but with R_{ext} ~562.9 mAW^{-1} at 800 nm and τ_{res} ~200 ms,[35] see Table 1.

Figure 9b plots R_{ext} as a function of wavelength from 490 up 870 nm. This follows the absorption of SLG/PVK films, Figure 7a, suggesting PVK is the main light absorbing layer in which photoexcited charges are supplied.[59] To get a better understanding of the spectral response of PDs versus wavelength, optical simulations are performed by extracting the PVK index from Ref. [134]. We use the PVK refractive index in transfer matrix calculations to estimate the absorption of SLG/PVK on our fibre structure. The imaginary and real part of the PVK average index are found by applying the Kramers-Kronig (KK) relation, $n_{PVK}(w) = 1 + 2\pi^{-1}\mathcal{P}\int_0^\infty w' K_{PVK}(w')/(w'^2 - w^2)\, dw'$, where $\mathcal{P}$ denotes the principal value of the integral and w is the angular f. The SLG refractive index is modelled by the Kubo conductance[135] at RT and E_F = 380 meV. The spectral response of the fibre PDs in Figure 9b follows the optical absorption of SLG/PVK on fibre in Figure 9b, i.e., drop of R_{ext} and absorption with increasing wavelength.

Mechanical characterizations are crucial to emulate real-life applications of wearable PDs.[26] These include washing in a tumble washing machine[6,136] and deformations against body motions (such as bending).[6] We thus test our fibre-based PDs according to AATCC[9] for washing. For mechanical deformations, we perform bending cycles, starting from a radius of curvature of 55 mm, where the PDs show almost no change, to 1 mm, where we observed degradation in our PDs.

Figure 10a is the schematic of a three-point bending setup (Deben Microtest) we use to characterise the effect of bending on the PD I_{ph}. The I_{ph} is first measured for no bending ($I_{ph, nobend}$), and then under bending ($I_{ph, bend}$). We use the ratio of ($I_{ph, bend}$) over ($I_{ph, nobend}$) to monitor the effect of mechanical deformations. The bending radius (R_b) is calculated as:[137]

$$R_b = \frac{[H^2 + (L/2)^2]}{2H} \qquad (9)$$

where H is the height at the chord midpoint of two ends of the arc, and L is the chord of circumference connecting two ends of the arc.

$I_{ph, bend}$/$I_{ph, nobend}$ shows up to ~15% and ~20% variation for R_b = 5 and 4 mm, respectively, Figure 10a. Figure 10b is a cross-

sectional image of fibre-based PDs. Figure 10c zooms-in the dashed square in Figure 10b, confirming that the interfaces between the functional layers are not affected even after bending to R_b = 5mm. Upon further bending (R_b <4 mm), $I_{ph, bend}$ drops to ~10% of $I_{ph, nobend}$, due to failure of various components, such as contact of Ag electrodes with graphene and crack formation in the fibre PD. Despite pushing our PDs to much lower R_b (4 mm) compared to InP-based semiconductor flexible PDs (R_b >38.1 mm),[138] we achieve 5 orders of magnitude higher R_{ext} (22,000 AW^{-1} here vs 0.12 AW^{-1} at 533 nm),[138] Table 1. Ref. [139] reported hybrid CVD SLG and PVK on Polyimide with R_b = 12 mm,[139] with one order of magnitude lower R_{ext} = 115 AW^{-1} at 515 nm[139] compared to ours. Ref. [140] fabricated PVK/Conjugated-Polymer composite PDs on PET with comparable R_b = 4 mm, but with 6 orders of magnitude lower R_{ext} ~154 mAW^{-1} at 835 nm,[140] see Table 1.

We then test our devices for a fixed R_b = 4 mm (as we observe ~20% variation in $I_{ph, bend}$/$I_{ph, nobend}$ up to R_b = 4 mm in Figure 10a) as a function of bending cycles, Figure 10d. After 100 bending cycles ($I_{ph, bend}$)/$I_{ph, nobend}$ changes<20%, Figure 10d. In similar conditions, Ref. [35] reported sixfold lower R_{ext} ~560 mAW^{-1} at 800 nm[35] for 60 less cycles, see Table 1.

We then test the PDs in a tumble washing machine according to the AATCC standard.[9] To prevent PVK oxidation and degradation during washing, two encapsulation approaches are used to protect the PDs. The fibres are conformally coated with ~1 µm parylene C, since this acts as a barrier to moisture[108] and gases.[108] The PDs are then further coated with (Polydimethylsiloxane) PDMS for additional waterproofing and resistance against tension/compression. Part A and B of the Si-based elastomer Polycraft T15 are mixed 1:1 using a speed mixer (DAC 150 FVZ-K) at 2000 rpm for 30s. The resulting solution is then spread on the fibre and cured at 80°C for 30 min to expedite the process and ensure cross-linking of polymer chains.[141] After encapsulation, the devices are tested at 488 nm at 1V. They have R_{ext} ~22,000 AW^{-1}', with no degradation. The I_{ph} of fibre-based PDs is first measured for no washing step ($I_{ph, nowash}$). The PDs are then placed in a tumble washing machine. The PDs are then drip dried in a ventilated oven at 60 °C (Genlab Air), then measured at various washing cycles ($I_{ph, wash}$) from 1 to 30, Figure 10e. After 20 cycles, the PDs show ~6% degradation in $I_{ph, wash}$/$I_{ph, nowash}$, Figure 10e. After 30 washing cycles, $I_{ph, wash}$/$I_{ph, nowash}$ drops ~28%, due to degradation of electrodes caused by stresses. Ref. [74] reported ~50% drop in drain current after 10 and 20 washing cycles, however, our fibre PDs maintained up to ~72% I_{ph} after 30 washing cycles.

3. Conclusion

We reported fibre-based SLG/PVK PDs with R_{ext} up to ~22,000 AW^{-1} at 1 V operating voltage at 488 nm. The PDs have a broad spectral responsivity between 488 and 870 nm, with rise and fall times ~9 and ~33 ms. The devices were subjected to mechanical bending tests (100 cycles at R_b ~4 mm) with $I_{ph, bend}$/$I_{ph, nobend}$ changes<10% and washing tests (AATCC standard) with $I_{ph, wash}$/$I_{ph, nowash}$ ~94% and ~72% at 20 and 30 cycles, respectively. The combination of high (~22 KAW^{-1}) responsivity, τ_{res}, flexibility, washability, and low (<1 V) operating voltage make our PDs attractive for wearable applications.

**ADVANCED
SCIENCE NEWS**

www.advancedsciencenews.com
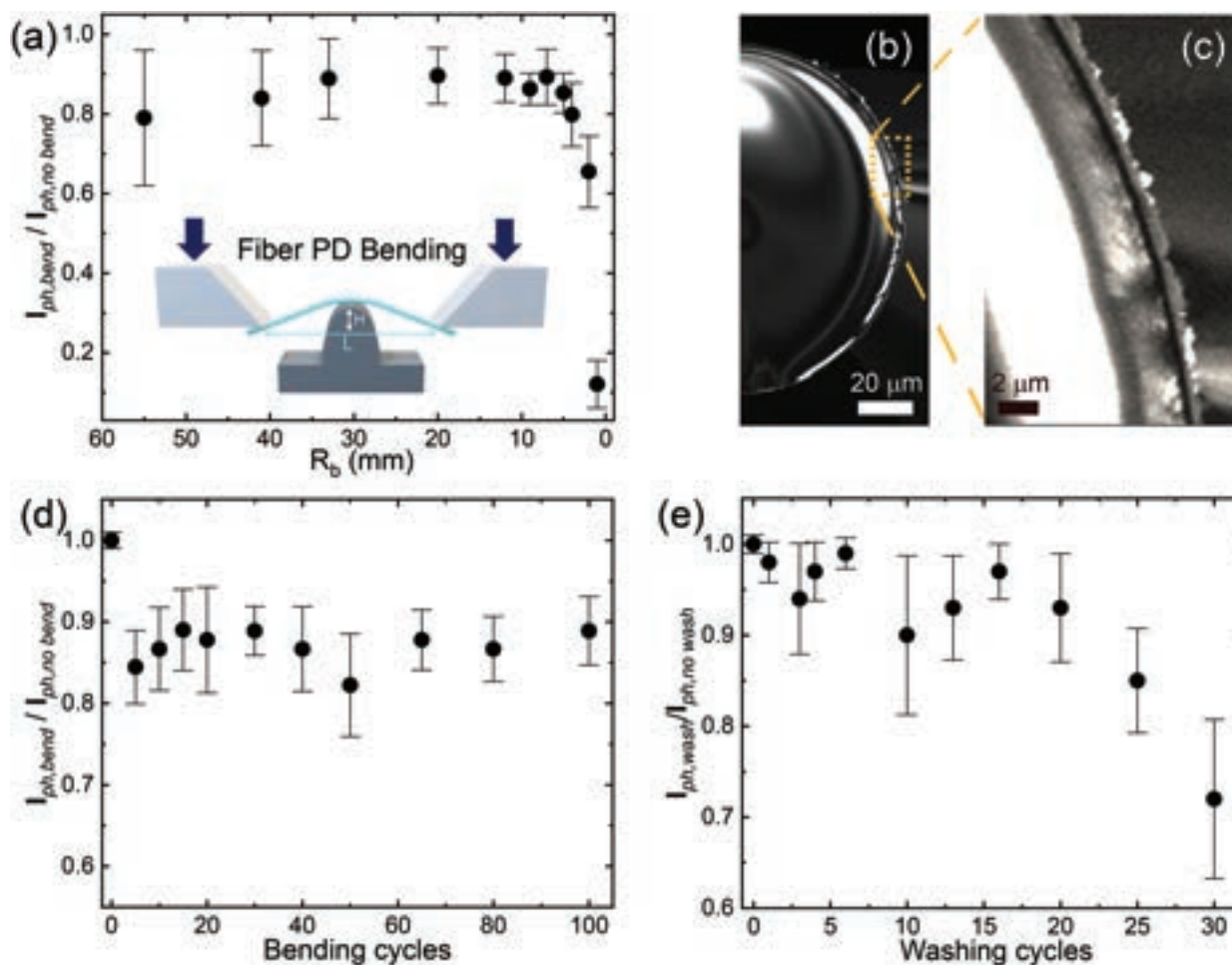
**ADVANCED
MATERIALS**

www.advmat.de

Figure 10. a) $I_{ph, bend}/I_{ph, nobend}$ for $N_R = 6$ as a function of R_b. b) Cross-section image of fibre-based PDs. c) Zoom-in of dashed square in (b) showing the device layers with no interface cracking or failure occurring between layers at $R_b = 5$ mm. d) $I_{ph, bend}/I_{ph, nobend}$ for $N_R = 6$ as a function of bending cycles for $R_b = 4$ mm. e) $I_{ph, wash}/I_{ph, nowash}$ for $N_R = 6$ as a function of AATCC washing cycles. At least five measurements are taken for each bending cycle, bending radius, or washing cycle, and the mean with standard deviation ($\pm$) is reported.

4. Experimental Section

CVD SLG is prepared on a 35 µm Cu foil as for Ref. [75]. The Cu foil is annealed up to 1000 °C for 30 min under H_2 at 20 sccm. Then, a gas mixture of CH_4 (5 sccm) and H_2 (20 sccm) is added to initiate growth at 1000 °C for 30 min. Finally, the sample is cooled in vacuum (1 mTorr) to RT.

A mixed-cation lead mixed-halide PVK is prepared by dissolving PbI_2 (1.2 M), formamidinium iodide (1.11 M), methylammonium bromide (0.21 M) and $PbBr_2$ (0.21 M) in a mixture of anhydrous dimethylformamide:dimethylsulfoxide (DMF:DMSO) (4:1 volume ratio) followed by 5 vol.% CsI stock solution (1.5 M in DMSO). The final solution is diluted by adding 50 vol.% DMF:DMSO (4:1 volume ratio).

Raman spectra are acquired at 514.5 nm using a Renishaw InVia with a 50 × objective < 0.1 mW.

For PDS measurement, a combination of a Light Support MKII 100 W Xe arc source and a CVI DK240 monochromator is used to produce a modulated monochromated light beam. The probe beam from a Qioptiq 670nm fibre-coupled diode laser directed parallel to the PVK film surface.

TRPL spectra are recorded at RT with a gated intensified CCD camera (Andor iStar DH740 CCI-010) connected to an Andor SR303i spectrometer with time resolution ~0.1 ns. A Ti:sapphire optical amplifier (1 kHz, 90 fs pulse width) is used to generate narrow bandwidth photoexcitation (FWHM = 10 nm at 400 nm) via a noncollinear optical parametric amplifier and a pulse fluence of 0.5 µJcm^{-2}.

Washability tests are conducted in a tumble washing machine (SKYLINE rotate washing color) at 40 °C up to 30 washing cycles, each programmed for 45 min, total volume ~0.37% (Persil detergent powder), and with ten 6 mm stainless steel balls.[9]

Statistical Analysis: For Raman analysis, at least 10 points are collected along the fibre in Figures 2 and 3 as mean, with standard deviation ($\pm$). In Figure 5 and Table 2 at least 5 points are collected as mean with standard deviation ($\pm$). The Raman spectra of Figure 2 are normalized to have the same I(G).

For bending and washability tests in Figure 10, at least 5 measurements are taken for each bending cycle, bending radius, or washing cycle, and the mean with standard deviation ($\pm$) was reported.

**ADVANCED
SCIENCE NEWS**

www.advancedsciencenews.com

**ADVANCED
MATERIALS**

www.advmat.de

Conflict of Interest

The authors declare no conflict of interest.

Data Availability Statement

The data that support the findings of this study are available from the corresponding author upon reasonable request.

Keywords

fibres, graphene, perovskites, photodetectors, wearables

[1] Y. Khan, A. E. Ostfeld, C. M. Lochner, A. Pierre, A. C. Arias, *Adv. Mater.* **2016**, *28*, 4373.

[2] M. K. Choi, J. Yang, K. Kang, D. C. Kim, C. Choi, C. Park, S. J. Kim, S. I. Chae, T. Kim, J. H. Kim, T. Hyeon, D.-H. Kim, *Nat. Commun.* **2015**, *6*, 7149.

[3] J. Wang, X. Li, Y. Zi, S. Wang, Z. Li, L. Zheng, F. Yi, S. Li, Z. L. Wang, *Adv. Mater.* **2015**, *27*, 4830.

[4] A. Nathan, A. Ahnood, M. T. Cole, S. Lee, Y. Suzuki, P. Hiralal, F. Bonaccorso, T. Hasan, L. Garcia-Gancedo, A. Dyadyusha, S. Haque, P. Andrew, S. Hofmann, J. Moultrie, D. Chu, A. J. Flewitt, A. C. Ferrari, M. J. Kelly, J. Robertson, G. A. J. Amaratunga, W. I. Milne, *Proc. IEEE* **2012**, *100*, 1486.

[5] L. Hu, M. Pasta, F. L. Mantia, L. Cui, S. Jeong, H. D. Deshazer, J. W. Choi, S. M. Han, Y. Cui, *Nano Lett.* **2010**, *10*, 708.

[6] W. Zeng, L. Shu, Q. Li, S. Chen, F. Wang, X. Tao, *Adv. Mater.* **2014**, *26*, 5310.

[7] A. M. Grancarić, I. Jerković, V. Koncar, C. Cochrane, F. M. Kelly, D. Soulat, X. Legrand, *J. Ind. Text.* **2018**, *48*, 612.

[8] M. Lou, I. Abdalla, M. Zhu, X. Wei, J. Yu, Z. Li, B. Ding, *ACS Appl. Mater. Interfaces* **2020**, *12*, 19965.

[9] *AATCC Testing Method, American Association of Textile Chemists and Colourists Technical Manual*, USA, **2004**.

[10] S. Rotzler, M. Krshiwoblozki, M. Schneider-Ramelow, *Text. Res. J.* **2021**, *91*, 2401.

[11] N. Karim, S. Afroj, S. Tan, P. He, A. Fernando, C. Carr, K. S. Novoselov, *ACS Nano* **2017**, *11*, 12266.

[12] I. G. Klepp, M. Buck, K. Laitala, M. Kjeldsberg, *Fash. Pract.* **2016**, *8*, 296.

[13] J. McCann, D. Bryson, *Smart clothes and wearable technology*, Elsevier, Amsterdam **2009**.

[14] S. Gupta, W. T. Navaraj, L. Lorenzelli, R. Dahiya, *npj Flex* **2018**, *2*, 8.

[15] M. Rein, V. D. Favrod, C. Hou, T. Khudiyev, A. Stolyarov, J. Cox, C. Chung, C. Chhav, M. Ellis, J. Joannopoul, Y. Fink, *Nature* **2018**, *560*, 214.

[16] W. Gao, S. Emaminejad, H. Y. Y. Nyein, S. Challa, K. Chen, A. Peck, H. M. Fahad, H. Ota, H. Shiraki, D. Kiriya, D. H. Lien, G. A. Brooks, R. W. Davis, A. Javey, *Nature* **2016**, *529*, 509.

[17] E. O. Polat, G. Mercier, I. Nikitskiy, E. Puma1, T. Galan, S. Gupta1, M. Montagut, J. J. Piqueras, M. Bouwens, T. Durduran, G. Konstantatos, S. Goossens, F. Koppens, *Sci. Adv.* **2019**, *5*, eaaw7846.

[18] M. Stoppa, A. Chiolerio, *J. Sens* **2014**, *14*, 11957.

[19] M. Tilli, M. Paulasto-Kröckel, M. Petzold, H. Theuss, T. Motooka, V. Lindroos, *Handbook of silicon based MEMS materials and technologies*, Elsevier, Amsterdam New York **2020**.

[20] A. S. Sedra, K. C. Smith, *Microelectronic circuits*, Oxford University Press, New York **1998**.

[21] G. Wang, C. Hou, H. Wang, *Flexible and Wearable Electronics for Smart Clothing*, John Wiley and Sons, New York **2020**.

[22] D. Son, J. Lee, S. Qiao, R. Ghaffari, J. Kim, J. E. Lee, C. Song, S. J. Kim, D. J. Lee, S. W. Jun, S. Yang, M. Park, J. Shin, K. Do, M. Lee, K. Kang, C. S. Hwang, N. Lu, T. Hyeon, D. H. Kim, *Nat. Nanotechnol.* **2014**, *9*, 397.

[23] R. Li, X. Xiang, X. Tong, J. Zou, Q. Li, *Adv. Mat.* **2015**, *27*, 3831.

[24] B. Dong, J. Hu, X. Xiao, S. Tang, X. Gao, Z. Peng, D. Zou, *Adv. Mat. Technol.* **2019**, *4*, 1900131.

[25] S. Kwon, H. Kim, S. Choi, E. G. Jeong, D. Kim, S. Lee, H. S. Lee, Y. C. Seo, K. C. Choi, *Nano Lett.* **2018**, *18*, 347.

[26] S. Cai, X. Xu, W. Yang, J. Chen, X. Fang, *Adv. Mater.* **2019**, *31*, 1808138.

[27] J. Allen, *Physiol. Meas.* **2007**, *28*, R1.

[28] X. Deng, Z. Li, F. Cao, E. Hong, X. Fang, *Adv. Funct. Mater.* **2023**, *33*, 2213334.

[29] Z. Li, T. Yan, X. Fang, *Nat. Rev. Mater.* **2023**, *8*, 587.

[30] Z. Wang, Z. Wang, D. Li, C. Yang, Q. Zhang, M. Chen, H. Gao, L. Wei, *Nature* **2024**, *626*, 72.

[31] X. Xu, J. Chen, S. Cai, Z. Long, Y. Zhang, L. Su, S. He, C. Tang, P. Liu, H. Peng, X. Fang, *Adv. Mater.* **2018**, *30*, 1803165.

[32] J. hui Chen, Q. Jing, F. Xu, Z. da Lu, Y. qing Lu, *Optica* **2017**, *4*, 835.

[33] J. Chen, Z. Liang, Z. Yuan, C. Li, M. Chen, Y. Xia, X. Zhang, F. Xu, Y. Lu, *Nanoscale* **2017**, *9*, 3424.

[34] F. Zhang, S. Niu, W. Guo, G. Zhu, Y. Liu, X. Zhang, Z. L. Wang, *ACS Nano* **2013**, *7*, 4537.

[35] H. Sun, W. Tian, F. Cao, J. Xiong, L. Li, *Adv. Mater.* **2018**, *30*, 1706986.

[36] S. M. Sze, K. K. Ng, *Physics of semiconductor devices*, John Wiley and Sons, New York **2006**.

[37] F. H. L. Koppens, T. Mueller, P. Avouris, A. C. Ferrari, M. S. Vitiello, M. Polini, *Nat. Nanotechnol.* **2014**, *9*, 780.

[38] B. E. A. Saleh, M. C. Teich, *Fundamentals of photonics*, John Wiley and Sons, New Jersey **2019**.

[39] X. Du, W. Tian, J. Pan, B. Hui, J. Sun, K. Zhang, Y. Xia, *Nano Energy* **2022**, *92*, 106694.

[40] S. Afroj, S. Tan, A. M. Abdelkader, K. S. Novoselov, N. Karim, *Adv. Func. Mater.* **2020**, *30*, 2000293.

[41] H. Jinno, K. Fukuda, X. Xu, S. Park, Y. Suzuki, M. Koizumi, T. Yokota, I. Osaka, K. Takimiya, T. Someya, *Nat. Energy* **2017**, *2*, 780.

[42] L. Wang, X. Fu, J. He, X. Shi, T. Chen, P. Chen, B. Wang, H. Peng, *Adv. Mater.* **2020**, *32*, 1901971.

[43] A. Satharasinghe, T. Hughes-Riley, T. Dias, *Sci. Rep.* **2018**, *8*, 1.

[44] A. C. Ferrari, F. Bonaccorso, V. Fal'ko, K. S. Novoselov, S. Roche, P Bøggild, S. Borini, F. H. L. Koppens, V. Palermo, et al., *Nanoscale* **2015**, *7*, 4598.

[45] F. Bonaccorso, Z. Sun, T. Hasan, A. C. Ferrari, *Nat. Photonics* **2010**, *4*, 611.

[46] J. Yoon, H. Sung, G. Lee, W. Cho, N. Ahn, H. S. Jung, M. Choi, *Energy Environ. Sci* **2017**, *10*, 337.

[47] A. Zanetta, et al., *Appl. Phys. Lett.* **2014**, 105.

[48] V. Sorianello, M. Midrio, G. Contestabile, I. Asselberghs, J. Van Campenhout, C. Huyghebaert, I. Goykhman, A. K. Ott, A. C. Ferrari, M. Romagnoli, *Nat. Photonics* **2018**, *12*, 40.

[49] M. Romagnoli, V. Sorianello, M. Midrio, F. H. L. Koppens, C. Huyghebaert, D. Neumaier, P. Galli, W. Templ, A. D'Errico, A. C. Ferrari, *Nat. Rev. Mater.* **2018**, *3*, 392.

[50] A. Tyagi, et al., *Nanoscale* **2022**, *14*, 2167.

[51] A. Giambra, V. Miseikis, S. Pezzini, S. Marconi, A. Montanaro, F. Fabbri, V. Sorianello, A. C. Ferrari, C. Coletti, M. Romagnoli, *ACS nano* **2021**, *15*, 3171.

[52] C. Backes, et al., *2D Mater.* **2020**, *7*, 022001.

[53] M. Khan, K. Indykiewicz, P. L. Tam, A. Yurgens, *Nanomaterials* **2022**, *12*, 331.

[54] S. D. Stranks, G. E. Eperon1, G. Grancini, C. Menelaou, M. J. P. Alcocer, T. Leijtens, L. M. Herz, A. Petrozza, H. J. Snaith, *Science* **2013**, *342*, 3341.

[55] S. De Wolf, J. Holovsky, S-J. Moon, P. Löper, B. Niesen, M. Ledinsky, F-J. Haug, J-H. Yum, C. Ballif, *J. Phys. Chem. Lett.* **2014**, *5*, 1035.

[56] N. J. Jeon, J. H. Noh, W. S. Yang, Y. C. Kim, S. Ryu, J. Seo, S. I. Seok, *Nature* **2015**, *517*, 476.

[57] J. Xing, Y. Zhao, M. Askerka, L. N. Quan, X. Gong, W. Zhao, J. Zhao, H. Tan, G. Long, L. Gao, Z. Yang, O. Voznyy, J. Tang, Z.-H. Lu, Q. Xiong, E. H. Sargent, *Nat. Commun.* **2018**, *9*, 1.

[58] D. P. McMeekin, G. Sadoughi, W. Rehman, G. E. Eperon, M. Saliba, M. T. Hörantner, A. Haghighirad, N. Sakai, L. Korte, B. Rech, M. B. Johnston, L. M. Herz, H. J. Snaith, *Science* **2016**, *351*, 151.

[59] L. Dou, Y. Yang, J. You, Z. Hong, W.-H. Chang, G. Li, Y. Yang, *Nat. Commun.* **2014**, *5*, 5404.

[60] F. Li, C. Ma, H. Wang, W. Hu, W. Yu, A. D. Sheikh, T. Wu, *Nat. Commun.* **2015**, *6*, 8238.

[61] C. Li, H. Wang, F. Wang, T. Li, M. Xu, H. Wang, Z. Wang, X. Zhan, W. Hu, L. Shen, *Light Sci. Appl.* **2020**, *9*, 1.

[62] W. Wang, D. Zhao, F. Zhang, L. Li, M. Du, C. Wang, Y. Yu, Q. Huang, M. Zhang, L. Li, J. Miao, Z. Lou, G. Shen, Y. Fang, Y. Yan, *Adv. Funct. Mater* **2017**, *27*, 1703953.

[63] M. Abdi-Jalebi, Z. Andaji-Garmaroudi, S. Cacovich, C. Stavrakas, B. Philippe, J. M. Richter, M. Alsari, E. P. Booker, E. M. Hutter, A. J. Pearson, et al., *Nature* **2018**, *555*, 497.

[64] F. P. G. de Arquer, A. Armin, P. Meredith, E. H. Sargent, *Nat. Rev. Mater* **2017**, *2*, 16100.

[65] T. M. Brenner, D. A. Egger, L. Kronik, G. Hodes, D. Cahen, *Nat. Rev. Mater* **2016**, *1*, 15007.

[66] J.-H. Choi, H. Wang, S. J. Oh, T. Paik, P. S. Jo, J. Sung, X. Ye, T. Zhao, B. T. Diroll, C. B. Murray, C. R. Kagan, *Nat. Rev. Mater.* **2016**, *352*, 205.

[67] L. Lin, J. Zhang, H. Su, J. Li, L. Sun, Z. Wang, F. Xu, C. Liu, S. Lopatin, Y. Zhu, K. Jia, S. Chen, D. Rui, J. Sun, R. Xue, P. Gao, N. Kang, Y. Han, *Nat. Commun.* **2019**, *10*, 1.

[68] D. De Fazio, D. G. Purdie, A. K. Ott, P. Braeuninger-Weimer, T. Khodkov, S. Goossens, T. Taniguchi, K. Watanabe, P. Livreri, F. H. L. Koppens, S. Hofmann, I. Goykhman, A. C. Ferrari, A. Lombardo, *ACS Nano* **2019**, *13*, 8926.

[69] R. R. Nair, P. Blake, A. N. Grigorenko, K. S. Novoselov, T. J. Booth, T. Stauber, N. M. R. Peres, A. K. Geim, *Science* **2008**, *320*, 5881.

[70] G. Konstantatos, M. Badioli, L. Gaudreau, J. Osmond, M. Bernechea, F. P. G. De Arquer, F. Gatti, F. H. Koppens, *Nat. Nanotechnol.* **2012**, *7*, 363.

[71] F. Xia, T. Mueller, Y.-M. Lin, A. Valdes-Garcia, P. Avouris, *Nat. Nanotechnol.* **2009**, *4*, 839.

[72] M. Saliba, T. Matsui, J.-Y. Seo, K. Domanski, J.-P. Correa-Baena, M. K. Nazeeruddin, S. M. Zakeeruddin, W. Tress, A. Abate, A. Hagfeldt, M. Grätzel, *Energy Environ. Sci.* **2016**, *9*, 1989.

[73] E. M. Tennyson, B. Roose, J. L. Garrett, C. Gong, J. N. Munday, A. Abate, M. S. Leite, *ACS Nano* **2018**, *13*, 1538.

[74] T. Carey, S. Cacovich, G. Divitini, J. Ren, A. Mansouri, J. M. Kim, C. Wang, C. Ducati, R. Sordan, F. Torrisi, *Nat. Commun.* **2017**, *8*, 220.

[75] S. Bae, H. Kim, Y. Lee, X. Xu, J. Park, Y. Zheng, J. Balakrishnan, T. Lei, H. R. Kim, Y. I. Song, Y. J. Kim, K. S. Kim, B. Ozyilmaz, J. H. Ahn, B. H. Hong, S. Iijima, *Nat. Nanotechnol.* **2010**, *5*, 574.

[76] F. Bonaccorso, A. Lombardo, T. Hasan, Z. Sun, L. Colombo, A. C. Ferrari, *Mater. Today* **2012**, *15*, 564.

[77] N. B. Babaroud, et al., *Microsyst. Nanoeng* **2022**, *8*, 107.

[78] K. Chatterjee, J. Tabor, T. K. Ghosh, *Fibers* **2019**, *7*, 51.

[79] A. C. Ferrari, J. Meyer, V. Scardaci, C. Casiraghi, M. Lazzeri, F. Mauri, S. Piscanec, D. Jiang, K. Novoselov, S. Roth, A. K. Geim, *Phys. Rev. Lett.* **2006**, *97*, 187401.

[80] A. C. Ferrari, D. M. Basko, *Nat. Nanotechnol.* **2013**, *8*, 235.

[81] A. C. Ferrari, *Solid State Commun.* **2007**, *143*, 47.

[82] A. Das, S. Pisana, B. Chakraborty, S. Piscanec, S. K. Saha, U. V. Waghmare, K. S. Novoselov, H. R. Krishnamurthy, A. K. Geim, A. C. Ferrari, A. K. Sood, *Nat. Nanotechnol.* **2008**, *3*, 210.

[83] D. M. Basko, S. Piscanec, A. C. Ferrari, *Phys. Rev. B* **2009**, *80*, 165413.

[84] L. G. Cançado, A. Jorio, E. H. M. Ferreira, F. Stavale, C. A. Achete, R. B. Capaz, M. V. O. Moutinho, A. Lombardo, T. S. Kulmala, A. C. Ferrari, *Nano Lett.* **2011**, *11*, 3190.

[85] M. Bruna, Anna K. Ott, M. Ijäs, D. Yoon, U. Sassi, A. C. Ferrari, *ACS Nano* **2014**, *8*, 7432.

[86] B. El-Kareh, L. N. Hutter, *Fundamentals of semiconductor processing technology*, Springer Science & Business Media, Berlin, Heidelberg **1995**.

[87] T. M. G. Mohiuddin, A. Lombardo, R. R. Nair, A. Bonetti, G. Savini, R. Jalil, N. Bonini, D. M. Basko, C. Galiotis, N. Marzari, K. S. Novoselov, A. K. Geim, A. C. Ferrari, *Phys. Rev. B* **2009**, *79*, 205433.

[88] D. Yoon, Y-W. Son, H. Cheong, *Phys. Rev. Lett.* **2011**, *106*, 155502.

[89] B. Fallahazad, K. Lee, G. Lian, S. Kim, C. M. Corbet, D. A. Ferrer, L. Colombo, E. Tutuc, *Appl. Phys. Lett.* **2012**, *100*, 093112.

[90] T. Gupta *Copper interconnect technology*, Springer Science & Business Media, Berlin, Heidelberg **2010**.

[91] S. Kim, J. Nah, I. Jo, D. Shahrjerdi, L. Colombo, Z. Yao, E. l Tutuc, S. K. Banerjee, *Appl. Phys. Lett.* **2009**, *94*, 062107.

[92] A. Stassen, R. De Boer, N. Iosad, A. Morpurgo, *Appl. Phys. Lett.* **2004**, *85*, 3899.

[93] S. S. Sabri, P. L. Lévesque, C. M. Aguirre, J. Guillemette, R. Martel, T. Szkopek, *Appl. Phys. Lett.* **2009**, *95*, 242104.

[94] L-L. Chua, J. Zaumseil, J-F. Chang, E. C-W. Ou, P. K-H. Ho, H. Sirringhaus, R. H. Friend, *Nature* **2005**, *434*, 194.

[95] Z. Yin, Z. Mai, Z. Liu, Y. Zhang, A. P. Zhang, Q. Zheng, *Adv. Sci.* **2018**, *5*, 1701041.

[96] T. Marszalek, M. Gazicki-Lipman, J. Ulanski, *Beil-stein J. Nanotechnol.* **2017**, *8*, 1532.

[97] R. L. Puurunen, *J. Appl. Phys.* **2005**, *97*, 9.

[98] J. D. Slinker, J. A. DeFranco, M. J. Jaquith, W. R. Silveira, Y-W. Zhong, J. M. Moran-Mirabal, H. G. Craighead, H. D. Abruña, J. A. Marohn, G. G. Malliaras, *Nat. Mater.* **2007**, *6*, 894.

[99] A. Kahouli, *J. Appl. Phys.* **2012**, *112*, 064103.

[100] M. S. Mathur, N. A. Weir, *J. Mol. Struct.* **1973**, *15*, 459.

[101] J. Jakabovic, J. Kovacac, M. Weisb, D. Haskoc, R. Srnaneka, P. Valenta, R. Reseld, *Microelectronics J.* **2009**, *40*, 595.

[102] J. Mark, K. Ngai, W. Graessley, L. Mandelkern, E. Samulski, G. Wignall, J. Koenig, *Physical properties of polymers*, Cambridge University Press, Cambridge **2004**.

[103] L. W. Ng, G. Hu, R. C. Howe, X. Zhu, Z. Yang, C. Jones, T. Hasan, *Printing of Graphene and Related 2D Materials*, Springer, Berlin, Heidelberg **2019**.

[104] J. Plummer, M. D. Deal, P. B. Griffin, *Silicon VLSI technology: fundamentals, practice and modeling*, Pearson Education India, Bengaluru **2009**.

[105] X. Liu, Y. Cheng, C. Liu, T. Zhang, N. Zhang, S. Zhang, J. Chen, Q. Xu, J. Ouyang, H. Gong, *Energy Environ. Sci.* **2019**, *12*, 1622.

[106] N. J. Jeon, J. H. Noh, Y. C. Kim, W. S. Yang, S. Ryu, S. I. Seok, *Nat. Mater.* **2014**, *13*, 897.

[107] T. A. Berhe, W.-N. Su, C.-H. Chen, C.-J. Pan, J.-H. Cheng, H.-M. Chen, M.-C. Tsai, L.-Y. Chen, A. A. Dubaleb, B.-J. Hwang, *Energy Environ. Sci.* **2016**, *9*, 323.

[108] K. Fukuda, T. Yokota, K. Kuribara, T. Sekitani, U. Zschieschang, H. Klauk, T. Someya, *Appl. Phys. Lett.* **2010**, *96*, 17.

[109] J. Zhou, Z. Liu, P. Yu, G. Tong, R. Chen, L. K. Ono, R. Chen, H. Wang, F. Ren, S. Liu, J. Wang, Z. Lan, Y. Qi, W. Chen, *Nat. Commun.* **2023**, *14*, 6120.

[110] M. Ledinsky, P. Loper, B. Niesen, J. Holovsky, S.-J. Moon, J.-H. Yum, S. De Wolf, A. Fejfar, C. Bal-lif, *J. Phys. Chem. Lett.* **2015**, *6*, 401.

[111] D. M. Calistru, L. Mihut, S. Lefrant, I. Baltog, *J. Appl. Phys.* **1997**, *82*, 5391.

[112] T. Dammak, N. Fourati, H. Boughzala, A. Mlayah, Y. Abid, *J. Lumin.* **2007**, *127*, 404.

[113] C. Quarti, G. Grancini, E. Mosconi, P. Bruno, J. M. Ball, M. M. Lee, H. J. Snaith, A. Petrozza, F. D. Angelis, *J. Phys. Chem. Lett.* **2013**, *5*, 279.

[114] M. Pazoki, A. Hagfeldt, T. Edvinsson, *Characterization Techniques for Perovskite Solar Cell Materials*, Elsevier, Amsterdam **2019**.

[115] Z. Zhu, J. Ma, Z. Wang, C. Mu, Z. Fan, L. Du, Y. Bai, L. Fan, H. Yan, D. L. Phillips, S. Yang, *J. Am. Chem. Soc.* **2014**, *136*, 3760.

[116] J. Li, S. Yuan, G. Tang, G. Li, D. Liu, J. Li, X. Hu, Y. Liu, J. Li, Z. Yang, et al., *ACS Appl. Mater. Interfaces* **2017**, *9*, 42779.

[117] Y. Lee, J. Kwon, E. Hwang, C. -H. Ra, W. J. Yoo. J. -H. Ahn, J. H. Park, J. H. Cho, *Adv. Mater.* **2015**, *27*, 41.

[118] Y. Wang, Y. Zhang, Y. Lu, W. Xu, H. Mu, C. Chen, H. Qiao, J. Song, S. Li, B. Sun, Y. Cheng, Q. Bao, *Adv. Opt. Mater.* **2015**, *3*, 1389.

[119] V. Lucarini, J. J. Saarinen, K. E. Peiponen, E. M. Vartiainen, *Kramers-Kronig relations in optical materials research*, Springer, Berlin, Heidelberg **2005**.

[120] W. Gannett, W. Regan, K. Watanabe, T. Taniguchi, M. F. Crommie, A. Zettl, *Appl. Phys. Lett.* **2011**, *98*, 24.

[121] D. Brida, A. Tomadin, C. Manzoni, Y. J. Kim, A. Lombardo, S. Milana, R. R. Nair, K. S. Novoselov, A. C. Ferrari, G. Cerullo, et al., *Nat. Commun.* **2013**, *4*, 1987.

[122] E. J. Santos, E. Kaxiras, *Nano Lett.* **2013**, *13*, 898.

[123] M. Lazzeri, S. Piscanec, F. Mauri, A. C. Ferrari, J. Robertson, *Phys. Rev. Lett.* **2005**, *95*, 236802.

[124] T. Mueller, F. Xia, P. Avouris, *Nat. Photonics* **2010**, *4*, 297.

[125] X. Gan, R-J. Shiue, Y. Gao, I. Meric, T. F. Heinz, K. Shepard, J. Hone, S. Assefa, D. Englund, *Nat. Photonics* **2013**, *7*, 883.

[126] A. Pospischil, M. Humer, M. M. Furchi, D. Bachmann, R. Guider, T. Fromherz, T. Mueller, *Nat. Photonics* **2013**, *7*, 892.

[127] X. Hu, X. Zhang, L. Liang, J. Bao, S. Li, W. Yang, Y. Xie, *Adv. Funct. Mater.* **2014**, *24*, 7373.

[128] C. Xie, P. You, Z. Liu, L. Li, F. Yan, *Light Sci. Appl.* **2017**, *6*, e17023.

[129] W. Zhang, C.-P. Chuu, J.-K. Huang, C.-H. Chen, M.-L. Tsai, Y.-H. Chang, C.-T. Liang, Y.-Z. Chen, Y.-L. Chueh, J.-H. He, M.-Y. Chou, L.-J. Li, *Sci. Rep.* **2014**, *4*, 3826.

[130] D. De Fazio, I. Goykhman, D. Yoon, M. Bruna, A. Eiden, S. Milana, U. Sassi, M. Barbone, D. Dumcenco, K. Marinov, A. Kis, A. C. Ferrari, *ACS Nano.* **2016**, *10*, 8252.

[131] M. I. Saidaminov, M. A. Haque, M. Savoie, A. L. Abdelhady, N. Cho, I. Dursun, U. Buttner, E. Alarousu, T. Wu, O. M. Bakr, *Adv. Mater.* **2016**, *28*, 8144.

[132] Y. Fang, A. Armin, P. Meredith, J. Huang, *Nat. Photonics* **2019**, *13*, 1.

[133] S. Bianconi, L. J. Lauhon, H. Mohseni, *Nat. Photonics* **2021**, *15*, 714.

[134] A. Tejada, S. Peters, A. Al-Ashouri, S. H. Turren-Cruz, A. Abate, S. Albrecht, F. Ruske, B. Rech, J. A. Guerra, L. Korte, *Adv. Opt. Mater* **2021**, *5*, 2101553.

[135] G. W. Hanson, *J. Appl. Phys.* **2008**, *44*, 084314.

[136] C. Mattmann, F. Clemens, G. Tröster, *Sensors* **2008**, *8*, 3719.

[137] J. W. S. Hearle, P. Grosberg, S. Backer, *Structural mechanics of fibers, yarns, and fabrics*, Wiley-Interscience, New York **1969**.

[138] W. Yang, H. Yang, G. Qin, Z. Ma, J. Berggren, M. Hammar, R. Soref, W. Zhou, *Appl. Phys. Lett.* **2010**, *96*, 121107.

[139] V. Q. Dang, G.-S. Han, T. Q. Trung, L. T. Duy, Y.-U. Jin, B.-U. Hwang, H.-S. Jung, N.-E. Lee, *Carbon* **2016**, *105*, 353.

[140] S. Chen, C. Teng, M. Zhang, Y. Li, D. Xie, G. Shi, *Adv. Mater.* **2016**, *28*, 5969.

[141] J. Park, S. Wang, M. Li, C. Ahn, J. K. Hyun, D. S. Kim, D. K. Kim, J. A. Rogers, Y. Huang, S. Jeon, *Nat. Commun.* **2012**, *3*, 1.